U.S.NRC
United States Nuclear Regulatory Commission
Protecting People and the Environment

RIL 2022-05

NRC TECHNICAL ASSESSMENT OF ZORITA MATERIALS TESTING RESULTS

Date Published: May 2022

Prepared by:
M. Hiser
P. Purtscher
R. Tregoning

Research Information Letter
Office of Nuclear Regulatory Research

Disclaimer

Legally binding regulatory requirements are stated only in laws, NRC regulations, licenses, including technical specifications, or orders; not in Research Information Letters (RILs). A RIL is not regulatory guidance, although NRC's regulatory offices may consider the information in a RIL to determine whether any regulatory actions are warranted.

TABLE OF CONTENTS

LIST OF FIGURES

LIST OF TABLES

EXECUTIVE SUMMARY

The purpose of this report is to review and assess the results from testing of irradiated stainless steel (SS) reactor internals harvested from the José Cabrera Nuclear Power Station (also known as Zorita) in Spain. The goal of this assessment is to briefly summarize the key results from this testing and succinctly identify relevant new information that may impact regulatory decisionmaking related to irradiation-assisted degradation of light-water reactor (LWR) vessel internals.

The Zorita reactor was a single-loop 160 megawatt-electric pressurized-water reactor (PWR) designed by Westinghouse Electric Corporation (Westinghouse) that achieved 26.4 effective full-power years of operation. The Zorita reactor internals were primarily composed of Type 304 austenitic SS. Harvesting from the Zorita internals included several pieces of SS baffle plate ranging from <1 to ~50 displacements per atom (dpa), as well as two pieces of core barrel SS weld ranging from <0.1 to ~2 dpa. The reactor internals were designed by Westinghouse and are very similar to Westinghouse-designed U.S. PWRs, which constitute the majority of the U.S. PWR fleet. These materials are some of the most representatively aged, high-fluence irradiated SS components that have been studied.

A number of research programs have been performed on the Zorita baffle plate and core barrel weld materials at a variety of laboratories in the U.S., Sweden, and Norway. The most significant results from the testing of Zorita baffle plate materials are the repeated observations of high crack growth rate (CGR) during irradiation-assisted stress corrosion cracking (IASCC) CGR testing and the very low amount of observed void swelling. The most significant results from the testing of Zorita weld materials are the very low fracture toughness (FT) values observed in multiple tests.

The Zorita baffle plate void swelling data should be taken as encouraging in that void swelling may not progress as rapidly in light water reactors (LWRs) as previously suggested. However, due to the lower operating temperatures of Zorita, the results cannot conclusively eliminate the potential for significant void swelling, particularly at higher doses and temperatures. The Zorita void swelling data show the strong influence of temperature, consistent with the results from other data in the literature. Industry and regulators should seek to observe additional LWR-irradiated materials at higher doses and temperatures near 360 degrees C to more confidently conclude that void swelling will not pose a significant issue during extended operating periods.

The Zorita baffle plate CGR data suggest that the IASCC CGR model for American Society of Mechanical Engineers (ASME) Code Case N-889 does not sufficiently predict the increased IASCC CGRs at fluences above 20 dpa observed in this material. This deficiency supports the proposed NRC condition on this Code Case, limiting its applicability to materials less than 20 dpa. Given the small volume of LWR internals exceeding 20 dpa, the practical implications of this condition are likely to be limited in the near term. When assessing the significance of the high CGRs on Zorita materials at high fluence levels, it should also be recognized that these data come from one heat of material irradiated in one reactor. Heat-to-heat variability can lead to significant uncertainty in materials testing, so additional CGR testing of highly irradiated materials should be pursued where practical to augment the Zorita plate testing data and confirm or refute the observations from the Zorita CGR testing.

The Zorita core barrel weld FT data should be carefully considered when assessing irradiated SS weld embrittlement, particularly given the very limited amount of data from in-service welds. The

Zorita data should be used to update existing guidance on irradiated SS weld FT as contained in BWRVIP-100, Revision 1, and WCAP-17096. Given the low susceptibility to IASCC, low operating stresses, and flaw-tolerant design of the BWR core shroud and PWR core barrel, it is not expected that these lower weld FT data pose an immediate safety concern. However, these results may necessitate reduced inspection intervals compared to previous guidance to ensure that an acceptable margin to structural integrity exists. Further research on irradiated SS weld materials should prioritize generating additional data at fairly low fluence levels (<2 dpa) and extend data on irradiated SS weld properties up to higher fluences approaching 20–30 dpa.

ABBREVIATIONS AND ACRONYMS

ADAMS	Agencywide Documents Access and Management System
ANL	Argonne National Laboratory
ASME	American Society of Mechanical Engineers
BWR	Boiling water reactor
BWRVIP	Boiling Water Reactor Vessel and Internals Project
CGR	Crack growth rate
EPRI	Electric Power Research Institute
FT	Fracture toughness
GB	Grain boundaries
HAZ	Heat-affected zone
HWC	Hydrogen water chemistry
IASCC	Irradiation-assisted stress corrosion cracking
INL	Idaho National Laboratory
LWR	Light water reactor
MRP	Materials Reliability Program
NEA	Nuclear Energy Agency
NWC	Normal water chemistry
OECD	Organization for Economic Co-operation and Development
PWR	Pressurized water reactor
PWSCC	Primary water stress corrosion cracking
RPV	Reactor Pressure Vessel
SCC	Stress corrosion cracking
SEM	Scanning electron microscopy
SMILE	Studsvik Materials Integrity for Life Extension
SS	Stainless steel
TEM	Transmission electron microscopy
WCAP	Westinghouse Commercial Atomic Power
ZIRP	Zorita Internals Research Project

CHAPTER 1: BACKGROUND ON ZORITA HARVESTING AND RESEARCH

The Zorita reactor operated from 1969 to 2006 with 26.4 effective full-power years of reactor operation. It was a single-loop 160 megawatt-electric pressurized-water reactor (PWR) designed by Westinghouse Electric Corporation (Westinghouse). Harvesting of reactor internals from the Zorita reactor was primarily carried out by the Zorita Internals Research Project (ZIRP), which was led by the Electric Power Research Institute (EPRI) and included cooperative funding from the NRC and other international organizations [1].

The Zorita reactor internals were primarily composed of Type 304 austenitic SS. Harvesting from the Zorita internals included several pieces of SS baffle plate ranging from <1 to ~50 displacements per atom (dpa), as well as two pieces of core barrel SS weld ranging from <0.1 to ~2 dpa. The reactor internals were designed by Westinghouse and are very similar to Westinghouse-designed U.S. PWRs, which constitute the majority of the U.S. PWR fleet. Therefore, the materials are highly representative of the SS internals in operating U.S. plants and may be used to validate (or refute) findings from other irradiated materials that may have experienced less representative aging or irradiation conditions, such as accelerated thermal aging or test reactor irradiation conditions with very high neutron fluxes or fast neutron spectrums.

1.1 Zorita-Related Research Programs

The initial harvesting of Zorita internals materials, including baffle plate and core barrel weld materials, as well as a three-dimensional fluence and temperature analysis (Materials Reliability Program (MRP) 392, “Materials Reliability Program: Zorita Internals Research Project: Radiation and Temperature Analysis of Zorita Baffle Plate and Core Barrel Weld Material” [2]), was performed under the ZIRP. EPRI led the multinational ZIRP project team, which included funding or in kind contributions from the NRC, Spanish Nuclear Safety Council (Spanish regulator), Swedish Radiation Safety Authority (Swedish regulator), Mitsubishi Heavy Industries (MHI), Axpo Holding (Swiss utility), and Tractebel (Belgian engineering consultancy). In addition to harvesting, ZIRP performed a thorough testing program of Zorita baffle plate materials at Studsvik (Swedish testing laboratory), covering tensile, irradiation assisted stress corrosion cracking (IASCC) crack initiation, IASCC crack growth, and fracture toughness (FT) (MRP-440, “Materials Reliability Program: Zorita Internals Research Project (MRP-440), Testing of Highly-Irradiated Baffle Plate Material” [1]). Additional in-kind effort for ZIRP performed by MHI included TEM to assess irradiation damage and void swelling. A follow-on program with a similar scope, funded by the NRC and EPRI at Studsvik, was performed and included optical microscopy, tensile, IASCC crack growth, and FT testing on Zorita core barrel weld materials (MRP-451, “Materials Reliability Program: Fluence Effects on Stainless Steel Welds (MRP-451): Crack Growth Rate and Fracture Toughness Testing of Zorita Weld and HAZ Materials” [3]).

To supplement the testing on as-received Zorita materials, in 2016, the NRC and EPRI supported the machining and shipment of baffle plate and core barrel specimens from Studsvik to the Halden Reactor in Norway to enable further irradiation of Zorita core barrel weld and heat-affected zone (HAZ) materials to generate data at higher fluences. The Halden reactor permanently shut down unexpectedly in 2018 before significant fluence could be acquired on the Zorita core barrel weld and HAZ samples. However, IASCC crack growth rate (CGR) tests were performed on a small number of Zorita baffle plate samples in the range of 40–50 dpa and core barrel weld and HAZ samples at 1–2 dpa (HWR-1236, “Final Report on the BWR Crack

Growth Rate Investigation IFA-791" [4] and HWR-1320, "Interim Report on the PWR Crack Growth Rate Investigation IFA-817" [5].

Following some observations of higher CGRs in the plate materials and low FT values in the Zorita weld/HAZ materials, the NRC funded the machining and shipping of two sets of additional specimens for independent testing at Argonne National Laboratory (ANL). These Zorita materials have been tested primarily for CGR and FT (results through 2019 are available in ANL 19/45, "Crack Growth Rate and Fracture Toughness Tests on Irradiated Ex-Plant Materials" [6]) as well as fractography and TEM (ANL-20/50, "Irradiated Microstructure of Zorita Materials" [7]). In addition, some of these materials have also been characterized for chemical composition by mass spectroscopy and TEM at Idaho National Laboratory (INL) to confirm they are typical Type 304 SS and assess potential transmutation effects at higher doses (INL/EXT-21-62220, "Chemical Compositional Analysis and Microstructural Characterization of Harvested Zorita Reactor Pressure Vessel (RPV) Internals" [8]).

In addition to the aforementioned testing programs that included NRC funding in cooperation with the EPRI MRP for PWR internals, EPRI also funded multiple projects, primarily through the Boiling Water Reactor Vessel and Internals Project (BWRVIP). Two key reports documenting BWRVIP testing of the Zorita materials are BWRVIP-294, Revision 2, "Fracture Toughness of Zorita RPV Core Internals Applicable to BWRs: Final Report 2019," issued October 2019 [9] and BWRVIP-335, "BWR Vessel and Internals Project, Crack Growth Rate Testing of Zorita Core Barrel Materials in BWR Environments," issued August 2020 [10]. The NRC does not have access to these data but has some awareness of a portion of the data through a conference publication [11]. Table 1 below provides a summary of the Zorita materials research programs, including funders, publications, scope, etc.

In the following sections, the authors summarize the key results from these testing programs and assess the major takeaways and relevance of the results for regulatory decisionmaking related to irradiation assisted degradation of LWR internals. Section 3 addresses significant results from the Zorita baffle plate materials, where high-fluence irradiation effects are the major focus. Section 4 addresses key results from the Zorita core barrel weld materials, which received lower fluence but, based on operating experience, represent a region that is more susceptible to cracking. Finally, Appendices A and B summarize the remainder of the results that are of lower importance to regulatory decisions for irradiation assisted degradation of LWR internals.

Table 1: Summary of Zorita Materials Research Programs

	ZIRP	Zorita Welds	Halden	ANL/INL	BWRVIP Testing
Funders	NRC, EPRI, and others	NRC and EPRI	Halden members	NRC	EPRI
Publications	MRP-440	MRP-451	HWR-1236 and HWR-1320	ANL-19/45, ANL-20/50 and INL/EXT-21-62220	BWRVIP-294, Rev. 2, and BWRVIP-335
Testing Location	MHI and Studsvik	Studsvik	Halden	ANL & INL	Studsvik
Materials	10, 25, 50 dpa plate	1, 2 dpa weld/HAZ	40–50 dpa plate, 1–2 dpa weld/HAZ	<1–50 dpa plate (<0.1–1 dpa weld also available)	1–2 dpa weld
Tensile Testing	X	X			unknown
Crack Initiation	X				unknown
CGR Testing	X	X	X	X	X
FT Testing	X	X		X	X
Optical / SEM	X	X	X	X	unknown
TEM	X		X	X	unknown
Composition				X	X

CHAPTER 2: DISCUSSION OF KEY RESULTS FROM ZORITA BAFFLE PLATE TESTING AND CHARACTERIZATION

The most significant results from the testing of Zorita baffle plate materials are the very low amount of observed void swelling and the repeated observations of high CGR during IASCC CGR testing. This section focuses on these results and a detailed assessment of their relevance to regulatory decisions. Appendix A to this report and MRP-440, ANL-19/45, and HWR-1320 provide a more comprehensive summary of the overall testing of Zorita baffle plate materials by the NRC and EPRI.

2.1 Overview of Zorita Plate Materials

Several pieces from the Zorita baffle plate were removed, covering a range of fluence from <1 to 50 dpa. The materials tested in the initial ZIRP program were targeted at 10, 25, and 50 dpa to assess the impact of fluence on microstructure and properties. The baffle plate was fabricated from 28.6-millimeter (mm)-thick plates of Type 304 SS. Documentation, such as certified material test report, on the base and weld metals used was not available. However, chemical analyses of Zorita plate specimens at INL [8] for the Zorita baffle plate materials showed that the composition was within the specifications of Type 304 SS (see Table 2).

Table 2: Zorita Plate Composition Compared to Type 304 SS Specification

	Carbon	Sulfur	Nitrogen	Chromium	Manganese	Nickel	Silicon	Phosphorus
Zorita Analysis	0.04%	0.02%	0.04%	19.7%	1.48%	9.85%	0.28%	0.02%
Type 304 SS Specification	0.08% max	0.03% max	0.10% max	18–20%	2% max	8–10.5%	0.75% max	0.045% max

The tensile testing results are shown in context with literature data in Appendix A. However, one important observation from the tensile testing was intergranular brittle failure in the room temperature air tensile test at 50 dpa. This is in contrast to the tensile tests performed at lower fluence levels and at higher temperatures, where ductile fracture behavior and fracture surfaces were observed. This intergranular brittle failure at 50 dpa indicates a change in ductility and failure mode due to increased fluence, which is important to highlight as it may help understand the increased IASCC CGR observed at higher fluence.

Figure 1 shows the trend with fluence and temperature for the yield stress and elongation after fracture for the nine air tensile tests across three fluence levels and two temperatures, with the highest dose specimens failing in a brittle fashion at much lower strain than the lower dose specimens at room temperature. Figure 2 shows the fracture surface from the room temperature tensile tests at ~25 and ~50 dpa, respectively. The 50-dpa fracture surface is almost completely intergranular and exhibited little necking, while all other samples showed ductile behavior: dimple fracture and significant necking.

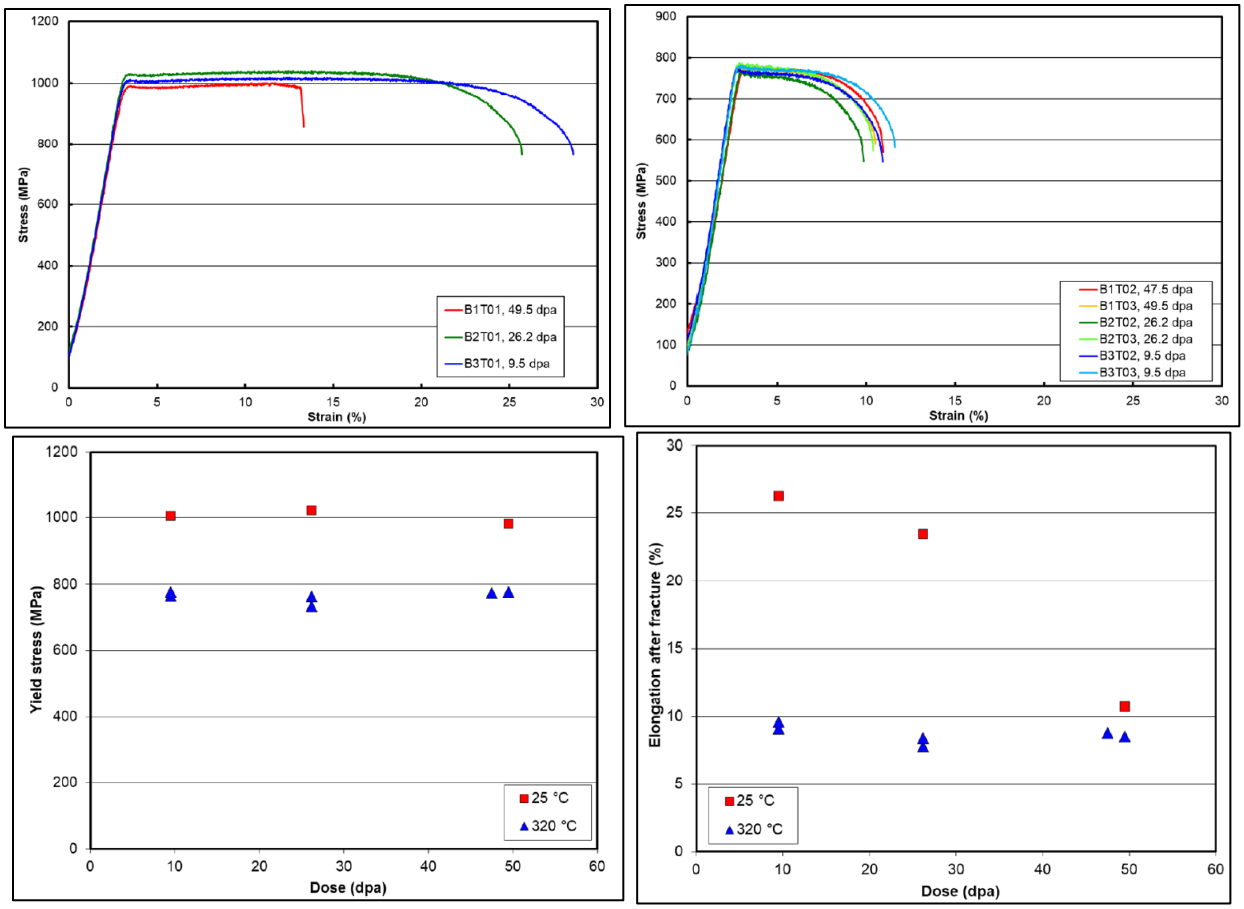

Figure 1: Top: Stress-strain curves for Zorita tensile specimens in air at three fluence levels and two temperatures: 25°C (left) and 320°C (right). Bottom: Yield stress (left) and elongation after fracture (right) as a function of fluence for Zorita tensile specimens in air at three fluence levels and two temperatures (Ref: Figures 4-4, 4-5, 8-1 and 8-2 from MRP-440)

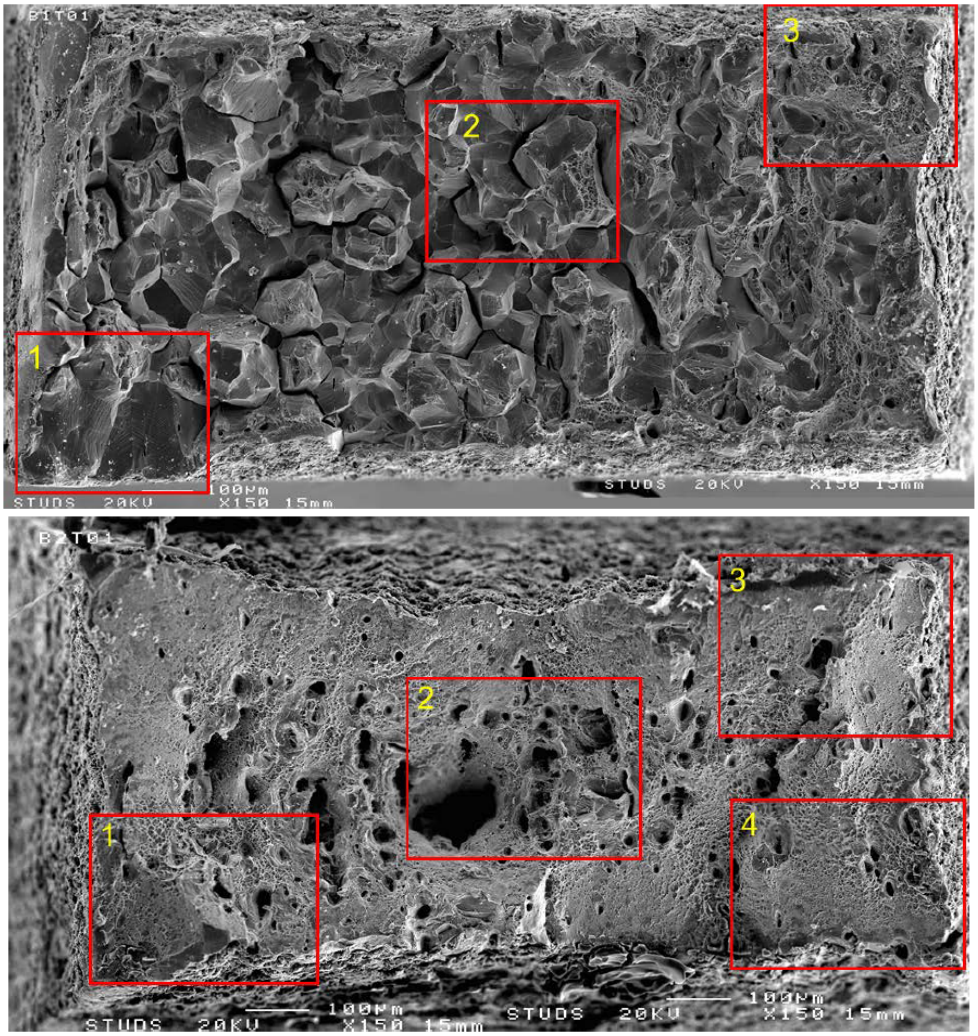

Figure 2: SEM fractography of fracture surfaces from 25 degrees C air tensile tests at 50 dpa (top) and 25 dpa (bottom). (Ref: Figures B-30 and B-47 from MRP-440.) Red boxes indicate locations of more detailed SEM images in MRP-440.

2.2 Crack Growth Rate Testing Results for Zorita Baffle Plate Materials

Researchers at a number of facilities have performed crack growth testing of Zorita baffle plate materials. Initially, the ZIRP project funded several CGR tests on Zorita plate materials ranging from 10 to 50 dpa at Studsvik. Next, a few samples ranging from 40 to 50 dpa were sent to Halden and tested as part of the Halden Reactor Project. Finally, two shipments of Zorita plate specimens (second shipment also included some Zorita weld specimens) were sent to ANL for independent testing funded by the NRC.

These tests have produced a significant amount of CGR data on Zorita plate materials in PWR and boiling water reactor (BWR) hydrogen water chemistry (HWC) environments, which are summarized in Figure 3. All data shown in Figure 3 were collected within valid stress intensity

factor (K) conditions.[1] and normalized to 320 degrees Celsius (C) in accordance with the IASCC CGR model from American Society of Mechanical Engineers (ASME) Code Case N-889, "Reference Stress Corrosion Crack Growth Rate Curves for Irradiated Austenitic Stainless Steels in Light Water Reactor Environments" [12,13]. In general, a single data point is reported for test segments where testing conditions remain consistent (e.g., environment, stress intensity factor, temperature). The data in Figure 3 show a bimodal CGR behavior in PWR/BWR HWC conditions, in which cracking progresses quite slowly for portions of the test before accelerating very rapidly by multiple orders of magnitude to higher CGRs (generally well beyond the IASCC CGR model in ASME Code Case N-889) during other portions of the test. The data in Figure 3 also shows that the likelihood of high CGR increases at higher fluences. Figure 4 provides an example of one of these higher CGR events, in this case Steps 18 and 19 from an ~50-dpa test. It should be noted that many of the lower CGR data ($<10^{-7}$ mm/second) in Figure 3 cover very little crack extension, which may indicate a lack of engagement of the crack, which is a common challenge when performing this type of testing. It should also be noted that in testing at ANL high CGRs were only observed when testing at elevated K levels > 25 MPa$\sqrt{m}$.

Testing has also been performed in BWR normal water chemistry (NWC) environments, with the results summarized in Figure 5. High CGRs are observed in BWR NWC conditions, with data above the IASCC CGR model from ASME Code Case N-889 in almost every instance. It should be noted that BWR internals are not expected to see fluences beyond 20–30 dpa [15], and nearly all U.S. BWRs now operate regularly with low-potential HWC conditions. Therefore, the applicability of BWR NWC data to operating plants at these high fluences is limited but nonetheless may be indicative or insightful of the IASCC susceptibility of these highly irradiated Zorita materials.

1. Valid stress intensity factor was determined based on ASTM E399 using an effective yield strength discounting 50% of the irradiation induced hardening as discussed by Jenssen et al. [14].

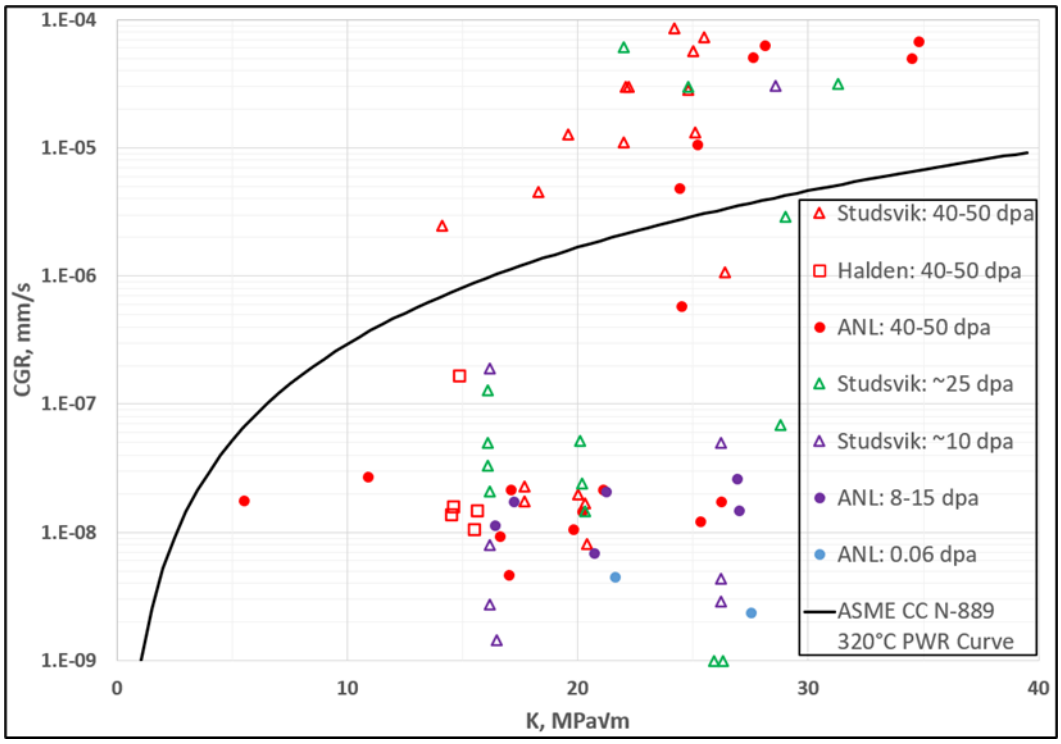

Figure 3: Summary of constant K IASCC CGR data as a function of stress intensity factor in PWR and BWR HWC conditions normalized to 320 degrees C compared to the IASCC CGR model curve from ASME Code Case N-889 for this temperature/chemistry

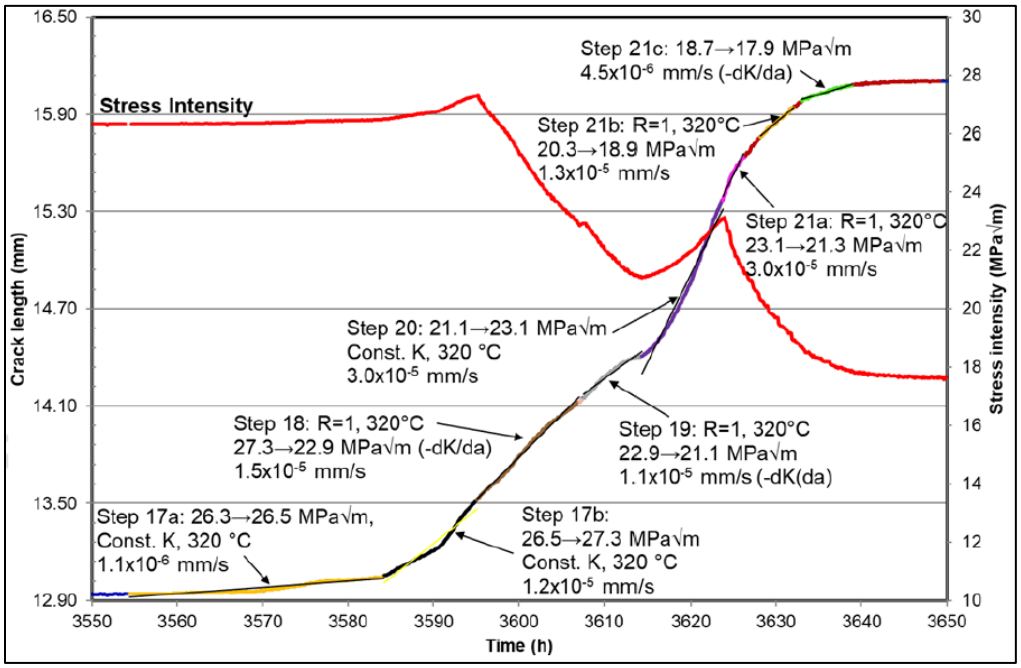

Figure 4: Crack length and stress intensity factor as a function of time during the IASCC CGR test on Specimen B1CT01 during Steps 17a through 21c (Ref: Figure 6-11 from MRP-440)

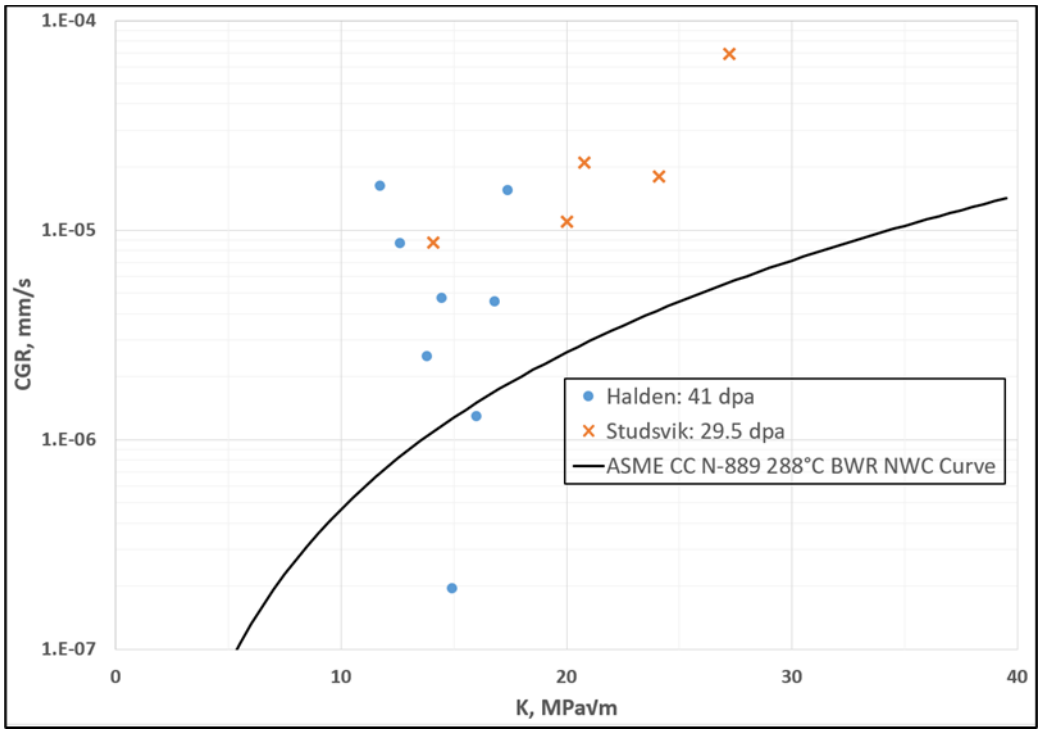

Figure 5: Summary of constant K IASCC CGR data as a function of stress intensity factor in BWR NWC conditions normalized to 288 degrees C compared to the IASCC CGR model curve from ASME Code Case N-889 for this temperature/chemistry

2.3 Representativeness of High Zorita CGRs

The high CGRs were developed under testing conditions that are representative of material behavior for reactor internals and therefore could occur if similar conditions arise in service. Based on the testing of the Zorita materials, the conditions that appear to lead to high CGRs are a K > 15 MPa√m combined with a fluence above 25 dpa. The following bullets summarize some of the factors that were considered in assessing the relevancy of the CGR results to operating plant conditions, while the sub-bullets provide context for what has been observed in the Zorita materials testing:

- Testing transients are representative of operating conditions.
  - In some cases, a modest transient such as a planned change in temperature (e.g., from 340 degrees C to 290 degrees C) or loading (e.g., transition from partial periodic unloading to constant K) or unplanned change in chemistry preceded an acceleration of the CGR by a few hours or days. However, there is no clear metallurgical explanation for why a modest change in temperature, loading, or chemistry should cause high CGR; changes of this magnitude routinely occur during plant operation.
  - These types of modest transients occur in primary water stress corrosion cracking (PWSCC) and IASCC CGR testing regularly without initiating high CGR.

  - There are also many examples in the Zorita CGR testing in which no apparent change in testing conditions precedes the initiation of high CGR. Therefore, the testing conditions are anticipated to be representative, including for the observed high CGR.

- Zorita CGR results are replicated at multiple laboratories and under multiple principal investigators using slightly different testing techniques and loading histories.

  - The high CGR behavior has been observed in many Zorita specimens tested at multiple laboratories with extensive experience in this type of testing, so it is not likely to be a result of an artifact of a certain testing approach by a particular investigator at a particular laboratory.

  - High CGRs have been observed even more consistently in testing in BWR NWC conditions, as shown in Figure 5, further supporting the idea that this is an inherent behavior of these highly irradiated materials.

  - The Zorita CGR tests were run in a similar manner to the way SCC CGR tests have been run historically on SS and nickel-based alloys for IASCC and PWSCC.

- K-validity criteria are met for most high CGR events.

  - All data have been analyzed for K validity consistent with accepted practices for irradiated SSs as discussed in Jenssen et al. [14], and most of the high CGR events occurred within K valid portions of the tests. The data presented in Figures 3 and 5 only include the K-valid portions of the tests, which include many high CGR events.

- Testing conditions during high CGR are representative of plant conditions.

  - EPRI and its contractors have proposed an explanation that high crack tip strain rates are the cause of the high CGR behavior and are not representative of reactor internals loading [1].

  - The EPRI explanation centers around the idea that during testing as CGR increases, insufficient load shedding occurs, leading to an increasing applied K that creates the high CGRs in an unrealistic manner relative to plant operations. It is true that in many instances, insufficient load shedding is observed during these high CGR events. However, this explanation has two key deficiencies:

    (1) The initiation and acceleration of high CGR occurs first without an increasing K (increases in K then happen in some cases because when high CGRs occur, it is challenging to decrease load quickly enough to maintain a constant K). EPRI's proposed explanation for the high CGRs does not explain what causes the initiation and acceleration of high CGR. The most plausible explanation appears to be the inherent stress corrosion cracking (SCC) susceptibility of the material.

    (2) In some instances, decreasing K loading has been successfully applied during testing once the high CGRs were observed (see Steps 18 and 19 in Figure 4). However, decreasing the applied K did not significantly decrease the high CGR.

2.4 Interpreting High CGRs on Zorita Materials

After extensive review of the Zorita CGR testing results from testing programs at Studsvik, Halden, and ANL, the most plausible explanation is that these high CGR data are representative of the IASCC susceptibility of these highly irradiated materials at elevated fluence. The high CGR events have been observed consistently across multiple specimens tested in multiple laboratories in a variety of environmental and loading conditions. Figure 6 shows the difference between observed IASCC CGR data in PWR conditions on Zorita materials and the IASCC CGR model prediction from ASME Code Case N-889 as a function of fluence. This plot clearly shows the increasing propensity for high CGR to occur at higher fluence levels, starting at about 25 dpa. It should be noted that the high CGR data tends to be about 5¬–50 times higher than the IASCC CGR model from ASME Code Case N-889 predicts, which can have a significant impact on how large flaws can grow unless they are detected by periodic inspections.

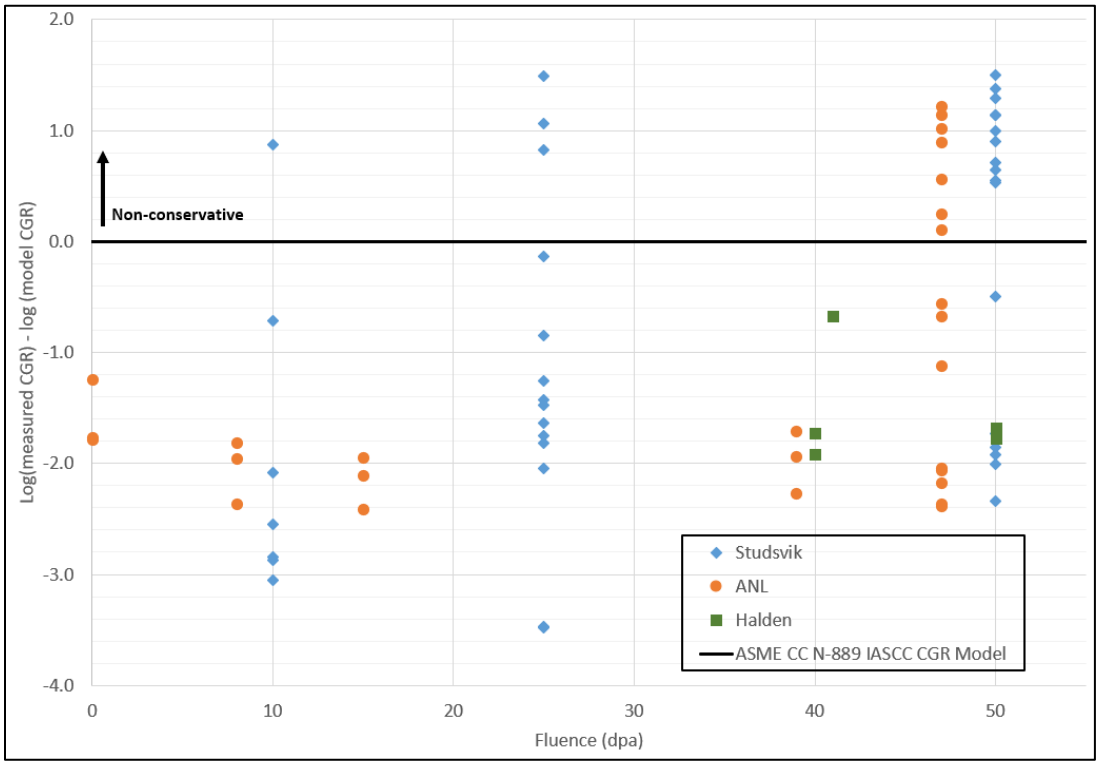

Figure 6: Summary of the Zorita CGR data in PWR conditions compared to the IASCC CGR model from ASME Code Case N-889 as a function of fluence

Researchers have made efforts to understand the microstructure of the Zorita materials to help explain this high CGR behavior [1,7,8]. The IASCC mechanism is understood to generally be driven by changes in microstructure due to radiation hardening and changes in microchemistry due to radiation-induced segregation at the grain boundaries (GBs) causing a decrease in local chromium content, allowing SCC to progress more easily [16]. It is possible that the high CGRs observed in the Zorita materials may be due to further progression of radiation-induced segregation or other aging mechanisms occurring locally at either the GBs or more generally in the material. Microstructural investigations on the Zorita materials have found an increase in

void fraction with increasing dose and temperature, although no clear evidence of an accumulation of voids at the GBs [7,8]. Other work on highly irradiated SSs has shown that voids can populate along the GBs and cause a GB weakening effect [17]. This GB weakening mechanism with increasing fluence is also consistent with the observation of intergranular brittle fracture in the 50-dpa air tensile test described previously. The combination of extensive radiation-induced segregation and GB weakening due to increasing voids provides a plausible explanation for the increasing susceptibility to higher CGRs with increasing fluence.

2.5 Implications of High CGRs from Zorita Plate Materials

This high CGR data from Zorita suggest that the IASCC CGR model for ASME Code Case N-889 may be insufficient to predict IASCC CGRs at fluences above 20 dpa. CGR data from other irradiated materials at fluence levels above 20 dpa are sparse and in general have been generated from less representative irradiation conditions, such as fast spectrum test reactors. The higher fluence data from Zorita, therefore, should be given considerable weight when assessing the structural integrity of reactor internals irradiated to high fluence (>20 dpa). Flaw evaluations performed on irradiated materials in this fluence that range above 20 dpa may need an additional safety factor beyond the IASCC CGR model for ASME Code Case N-889 to account for the observed high CGRs from the Zorita materials (which were not included in the development of the IASCC CGR model for ASME Code Case N-889).

Consistent with these observations, NRC staff have proposed three conditions on Code Case N-889 in draft Regulatory Guide DG-1367, “Inservice Inspection Code Case Acceptability, ASME Section XI, Division 1.” [18] The first condition limits the applicability of the Code Case to fluence levels less than 20 dpa. The remaining two conditions address deficiencies in the Code Case at predicting CGRs at low fluence levels below 0.75 dpa and with predicting irradiated yield stress for cold-worked non-molybdenum bearing SSs.

Other factors to consider are that highly irradiated internals components tend to experience very low operational stresses during normal operation, and irradiation-induced stress relaxation tends to reduce fit up or residual stresses from fabrication/construction. These factors may mitigate the effects of susceptibility to higher CGRs by minimizing the applied stresses that drive crack growth.

It should also be recognized that the data are from probably only one heat of material irradiated in one reactor. Heat to-heat variability is a known phenomenon in materials testing, so additional CGR testing of highly irradiated materials should be pursued where practical to augment the Zorita plate testing data and confirm or refute the observations from the Zorita CGR testing. The OECD/NEA SMILE project, running from 2021 to 2025, plans to harvest and test Type 304 SS internals materials from the Ringhals 2 PWR with fluences up to 50 dpa. The SMILE data should help to provide additional understanding of the IASCC behavior of high-fluence PWR internals.

2.6 Void Swelling Evaluation from Transmission Electron Microscopy

As part of the ZIRP project, Mitsubishi Heavy Industries performed detailed TEM on the high dose (50 dpa) sample. This TEM work provided information on various characteristics of irradiation damage, including precipitates, Frank loops, hardness, gas generation, and void swelling. Of particular interest were estimates of void swelling, which has been proposed as a potential life-limiting aging mechanism in irradiated SSs [19]. Figure 7 shows an example TEM

image from the highest swelling location. The three TEM images to the right side of Figure 7 show the visual fields analyzed for swelling (voids appear as hazy circles).

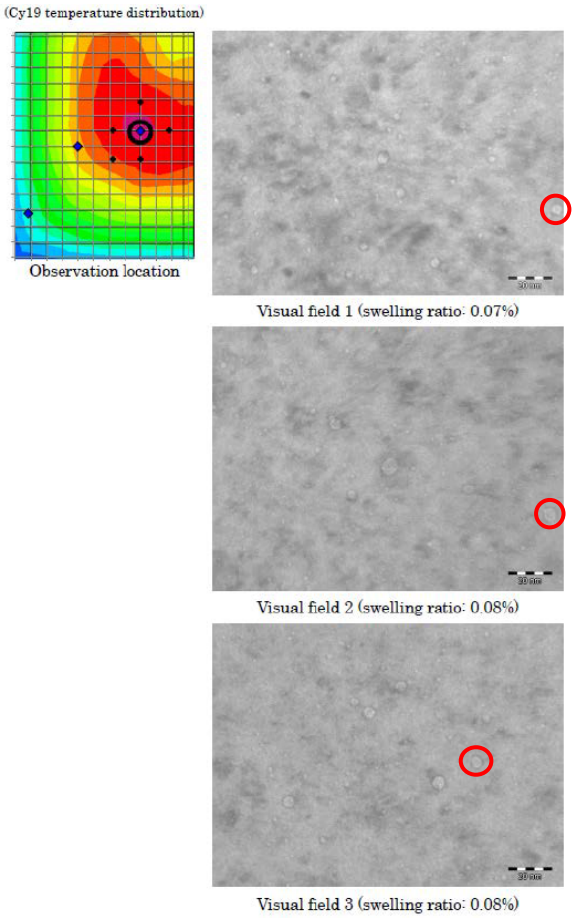

Figure 7: Swelling observations for highest temperature location from Zorita baffle plate material. Examples of voids or bubbles shown in red circles. (Ref: Figure F-26 from MRP-440)

The void swelling mechanism in SSs is complex and sensitive to a number of factors, including dose, dose rate, irradiation temperature, and neutron energy spectrum. Past observations of void swelling from fast reactors should be interpreted cautiously because the irradiation conditions can differ in the following important respects from those from LWRs:

- **Irradiation temperature:** Void swelling is known to increase strongly with increasing temperature [16]. Fast reactor data on void swelling have shown significant swelling at temperatures above 400 degrees C [19]. Peak temperatures in LWR internal components (accounting for gamma heating) are calculated to be about 360 degrees C, with most of the internals at lower temperatures than 360 degrees C [19].

- **Neutron energy spectrum:** Thermal neutrons tend to generate helium gas in SS during irradiation. Helium has been shown to help voids stabilize and grow more readily, causing an increase in void swelling. Therefore, the neutron energy spectrum (fast only or mixed as in an LWR) influences the generation of helium gas and the rate of swelling. From a neutron energy spectrum perspective, fast reactor irradiation conditions (which

lack a significant thermal neutron flux) would tend to produce less swelling than LWR irradiation conditions [19].

- **Dose rate:** Higher dose rate generally causes the onset of significant swelling at a higher dose [16,19]. Therefore, for a given dose (fluence), swelling is negatively correlated to dose rate (more swelling with a lower dose rate). Fast reactor irradiations generally create a much higher dose rate than LWR service conditions, so fast reactor irradiations will tend to underpredict swelling at a given dose based on their higher dose rates.

Based on these multiple competing factors that differ between fast reactors and LWRs, the results of void swelling from high-dose LWR-irradiated materials are particularly insightful for understanding how void swelling may progress during extended LWR operation. The top part of Figure 8 shows the results from the TEM analyses of void swelling in the Zorita materials, which indicate very low levels of void swelling (<0.08 percent) in all observed locations, including both the maximum temperature and maximum fluence locations (note the maximum temperature and fluence occur in different locations). The bottom part of Figure 8 shows that the Zorita swelling results correlate much more strongly with temperature than with dose, consistent with the data trends shown in the literature [19].

2.7 Implications of Void Swelling Results from Zorita Plate Materials

It should be noted that the Zorita reactor operated at a slightly lower temperature than many U.S. PWRs. Specifically, the maximum temperature was <330 degrees C in the Zorita internals, while many U.S. PWRs are expected to see internal components with peak temperatures near 360 degrees C. These data should therefore be taken as an encouraging sign that void swelling may not progress as rapidly in LWRs as previously suggested [19], but not conclusively to eliminate the potential for significant void swelling, particularly at higher doses and temperatures. Even the Zorita void swelling data show a strong influence of temperature as seen in Figure 8.

After previously expecting void swelling to reach a steady-state rate of 1% per dpa based on data at higher temperatures, more recently [20] has determined that a maximum steady-state swelling rate of 0.07% per dpa (after the incubation period) is more likely for LWR conditions. This appears to be consistent with the fairly low swelling observed in the Zorita materials. Nevertheless, industry and regulators should seek to observe additional LWR irradiated materials at higher doses and temperatures near 360 degrees C to more confidently conclude that void swelling will not pose a significant issue during extended operating periods.

Analysis location	Irradiation dose [dpa]	Irradiation temperature* [°C]	Swelling ratio			Reference film thickness [nm]
			Per visual field		Average	
①	39	319	1	0.05%	0.04%	75
			2	0.03%		66
			3	0.04%		74
②	34	327	1	0.07%	0.07%	73
			2	0.08%		74
			3	0.08%		64
③	35	327	1	0.09%	0.08%	68
			2	0.07%		69
			3	0.08%		67
④	37	324	1	0.06%	0.05%	57
			2	0.04%		57
			3	0.05%		67
⑤	33	326	1	0.04%	0.07%	64
			2	0.10%		48
			3	0.10%		42
⑥	36	325	1	0.05%	0.05%	54
			2	0.05%		63
			3	0.06%		63
⑦	36	325	1	0.10%	0.07%	52
			2	0.07%		82
			3	0.06%		72
⑧	33	326	1	0.06%	0.06%	74
			2	0.05%		764
			3	0.06%		67
⑨	47	299	1	0.02%	0.02%	71
			2	0.02%		70
			3	0.01%		71

*Maximum temperature for Cycle 19

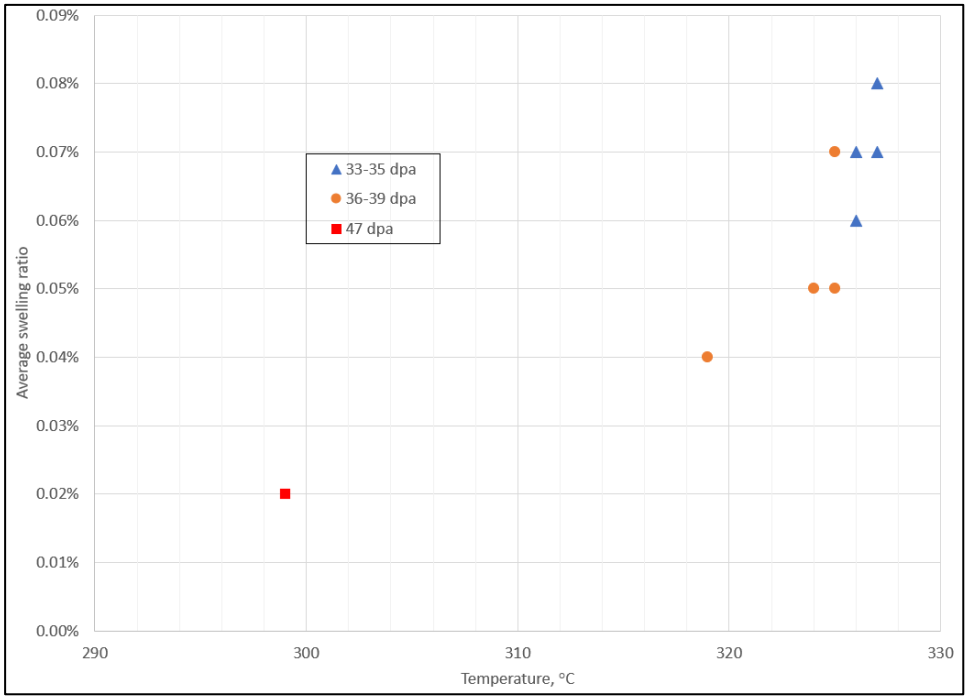

Figure 8: Top: Summary table of Zorita void swelling results (Ref: Table F-5 from MRP-440); bottom: Zorita void swelling results plotted as a function of temperature

CHAPTER 3: DISCUSSION OF KEY RESULTS FROM ZORITA CORE BARREL WELD TESTING AND CHARACTERIZATION

The most significant results from the testing of Zorita weld materials are the very low FT values observed in multiple tests. This section details these results and assesses their relevance to regulatory decisions. Appendix B and MRP-451 and BWRVIP-335 provide a more comprehensive summary of the overall testing of Zorita weld and HAZ materials by the NRC and EPRI [3,10].

3.1 Overview of Zorita Weld and Heat-Affected Zone Materials

Two separate welds from the Zorita core barrel were removed. Weld 1 was extracted from an axial (vertical) core barrel weld towards the top of active fuel and had a maximum fluence of ~1 dpa (also used in BWRVIP testing). Weld 2 was harvested from an axial (vertical) core barrel weld at the core midplane and includes an intersection with a circumferential (horizontal) weld. Weld 2 had a maximum fluence of ~2 dpa. The materials tested in the EPRI-NRC program ranged in dose from 0.7 to 1.9 dpa. The core barrel was fabricated from 45-mm-thick plates of Type 304 SS. Metallographic samples from both welds showed that the measured ferrite contents were in the range of 5–7 percent, which is normal for SS welds. Documentation (such as certified material test report) on the base and weld metals used was not available. However, chemical analyses of each of the two welds were typical for Type 308 weld metal, as shown in Table 3 [11].

Table 3: Chemical Analysis Results from the Zorita Weld Metal [11]

	Carbon	Manganese	Sulfur	Chromium	Iron	Nickel	Molybdenum	Copper
Zorita Analysis	0.06%	1.47%	0.017%	21.5%	70.5%	9.9%	0.04%	0.13%
Type 308 SS Specification	0.08% max	1.0-2.5%	0.03% max	19.5-22.0%	Balance	9.0-11.0%	0.75% max	0.75% max

3.2 Fracture Toughness Testing Results for Zorita Weld and Heat-Affected Zone Materials

FT testing of Zorita weld and HAZ materials in air and PWR environments has been performed at Studsvik according to ASTM E1820 through a cooperatively funded project by the NRC and EPRI. Additional FT tests have also been performed at Studsvik under BWR conditions with separate EPRI funding [11]. Figure 9 shows the Zorita weld and HAZ FT testing results as a function of test temperature.

The Zorita weld metal tests displayed low FT such that a stable J-integral vs. crack growth resistance (J-R) curve was not able to be constructed and work per unit of fracture surface area (J) at 1 mm crack extension could not be reported.[2] [3]. Unstable crack advance occurred in all these specimens; therefore, the linear-elastic fracture mechanics test standard ASTM E399 was used to evaluate the data instead. As seen in Figure 9, there were no significant effects of temperature, dose, or test environment on the Zorita weld metal FT over the range of conditions

2. EPRI has indicated that they are working to develop J-R curves to better analyze these FT tests [21].

evaluated. Some of the fracture surfaces of low-toughness Zorita weld specimens show fine-scale dimpled features, suggesting that the low toughness may be associated with the size and distribution of particles, such as inclusions that formed on initial solidification of the weld. Figure 10 compares the Zorita weld FT data to that in the literature and shows clearly that the Zorita weld FT data values are much lower than those from the limited data in the literature at similar fluences.

In contrast to the weld metal tests, FT testing of the HAZ resulted in increased resistance to ductile tearing in comparison with the weld material, and J-R curves were constructed. An effect of dose and environment on the measured J at 1 mm was observed. From power law curve fits (i.e., $J = C (\Delta a)^n$) to the data, the value of coefficient C decreased from ~300 kilojoules per square meter (kJ/m^2) at ~0.7 dpa in air to ~200 kJ/m^2 at ~1.5 dpa in a PWR environment as shown in Figure 11. Figure 12 shows that the Zorita HAZ FT was relatively low but, unlike the weld metal data, it fell within the observed range of literature data for HAZ and base metal.

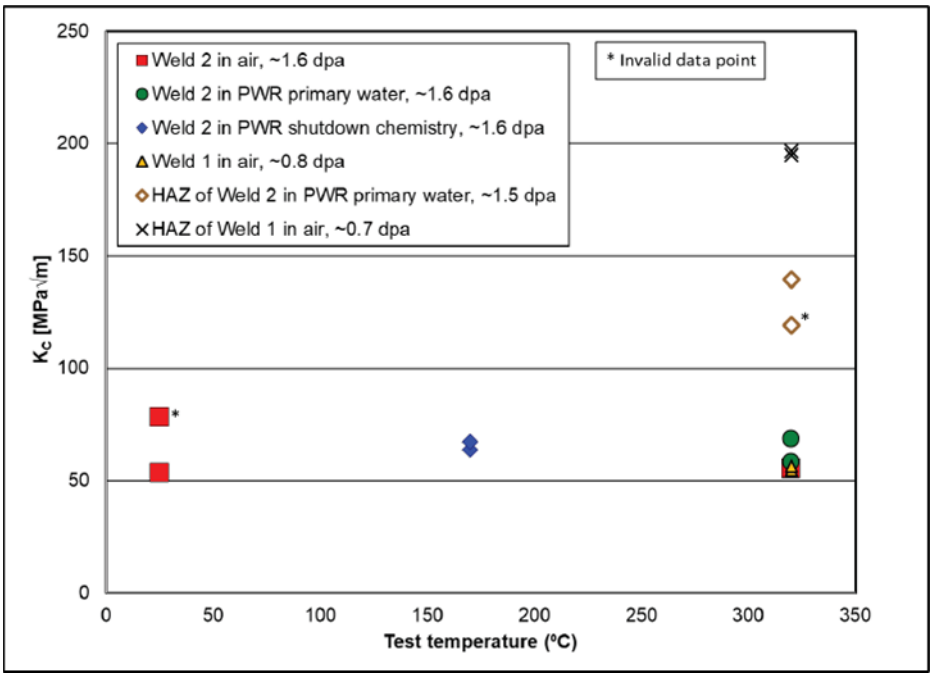

Figure 9: Summary of FT test results on Zorita weld and HAZ materials (Ref: Figure 7-12 from MRP-451)[3]

3. FT is expressed as Kc, which is calculated the same as KJc in ASTM E1921.

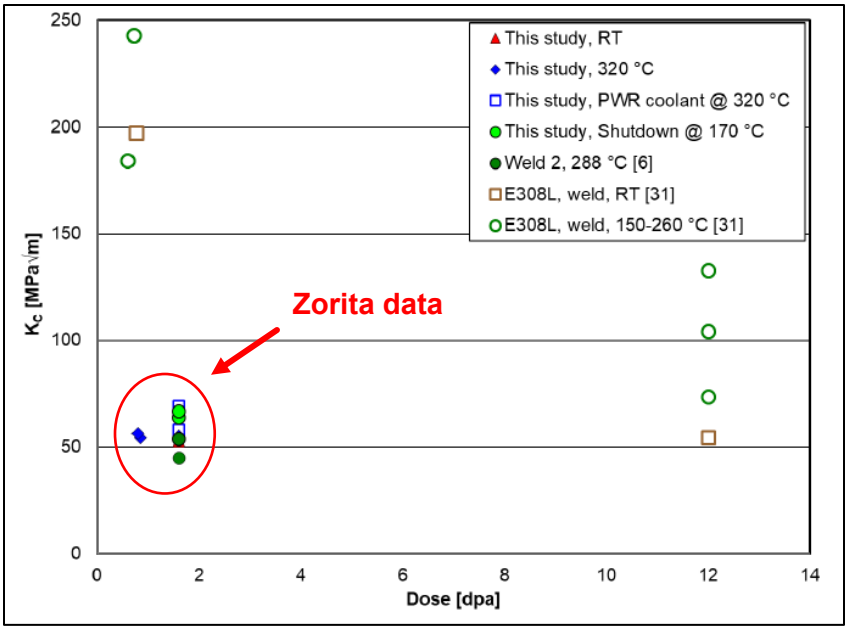

Figure 10: Summary of Zorita weld FT data as a function of dose compared to the data in the literature on irradiated SS weld FT (Ref: Figure 7-14 from MRP-451)[3, 4]

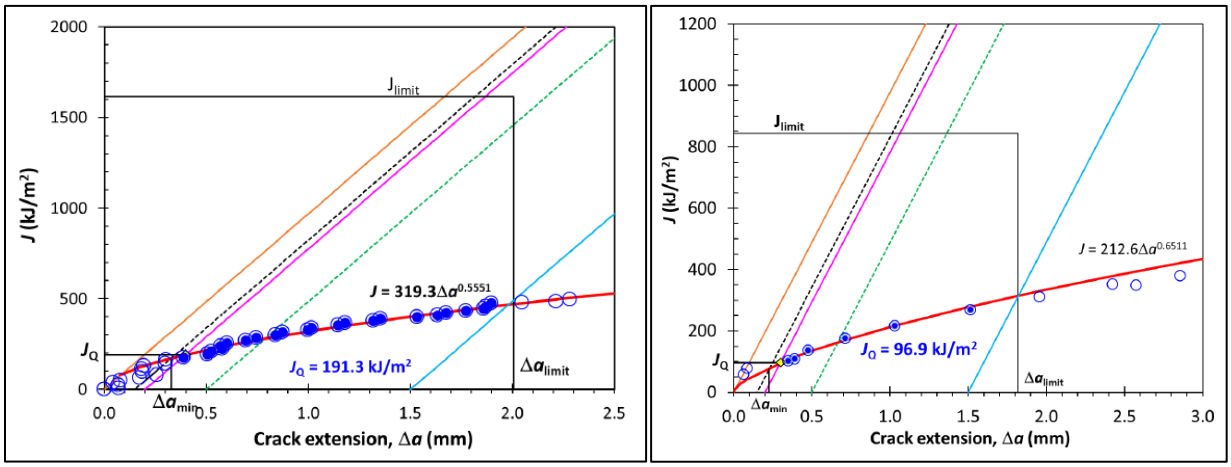

Figure 11: J-R curves for selected Zorita HAZ specimens. Left: W1HCT04 at ~0.7 dpa tested in air at 320 degrees C Right: W2HCT06 at ~1.5 dpa tested in PWR primary water at 320 degrees C (Ref: Figures 6-4 and 6-12 from MRP-451)[3]

4 Please refer to Appendix D for citations shown in this figure.

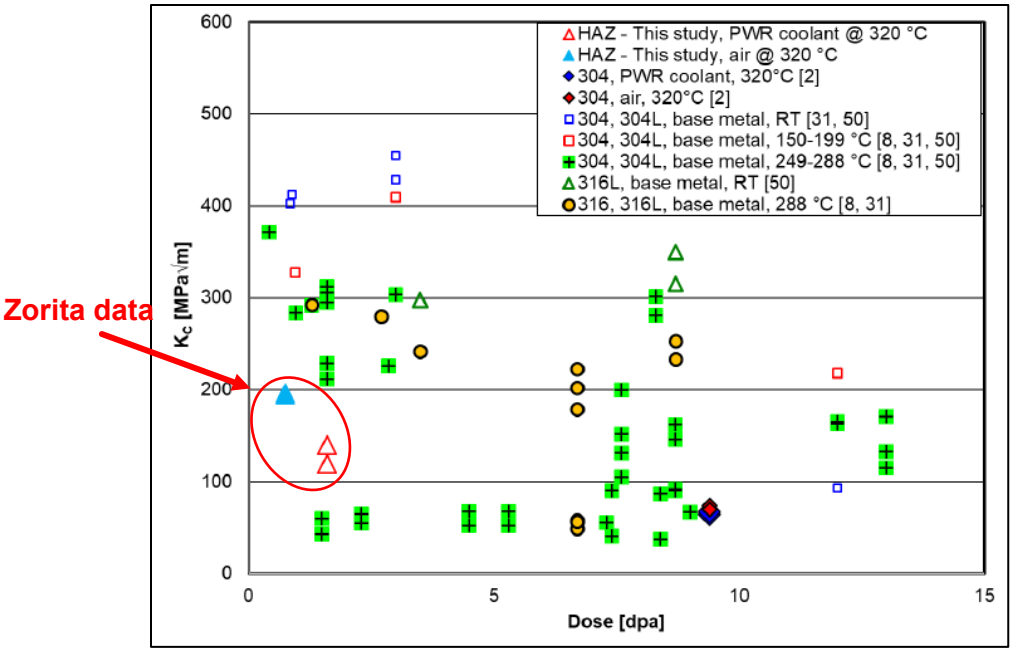

Figure 12: Summary of Zorita HAZ FT data as a function of dose compared to the data in the literature on irradiated SS HAZ and base metal FT (Ref: Figure 7-15 from MRP-451)[3,4]

3.3 Implications of Low Fracture Toughness for Zorita Weld Materials

Based on Figures 10 and 12, the most significant results from this testing are the very low FT results for the weld metals. There are very limited data on irradiated SS weld materials, and the Zorita welds are representative of the SS welds that are in operating U.S. reactors. Therefore, these new data should be carefully considered to determine whether past assumptions about irradiated SS weld FT are still appropriate. The NRC has approved using the criteria in BWRVIP-100, Revision 1-A, "BWR Vessel and Internals Project, Updated Assessment of the Fracture Toughness of Irradiated Stainless Steel for BWR Core Shrouds," issued February 2017 [22] for irradiated SS weld FT to assess flaws in BWR core shrouds. Identical values for FT in irradiated SSs are also contained in Westinghouse Commercial Atomic Power (WCAP)-17096, Revision 2, "Reactor Internals Acceptance Criteria Methodology and Data Requirements," issued 2006 [23], which is referenced in MRP-227. Revision 1-A, "Materials Reliability Program: Pressurized Water Reactor Internals Inspection and Evaluation Guidelines," issued December 2019 [24]. On March 22, 2021, EPRI notified the NRC by letter [25] of a notification under Title 10 of the *Code of Federal Regulations* Part 21, "Reporting of Defects and Noncompliance," [26] sent to the industry about the potential nonconservatism in BWRVIP-100, Revision 1-A (EPRI, 2017). During a public meeting on May 27, 2021, Westinghouse and the Pressurized Water Reactor Owners Group further indicated that they were assessing "if there is an impact on the flaw tolerance methodologies and/or fracture toughness values in WCAP-17096-NP-A, Rev. 2 and WCAP-17096-NP, Rev. 3." [28] Finally, in November 2021, the NRC released publicly an assessment [29], following the process in LIC-504, Revision 5, "Integrated Risk-Informed Decisionmaking Process for Emergent Issues," issued March 2020 [30], of the nonconservatism issue in BWRVIP-100, Revision 1-A. The assessment concluded that while there was not an immediate safety issue, this issue should be monitored through the NRC inspection program to confirm industry addresses it appropriately.

Figure 13 shows a plot of the Zorita weld and HAZ FT data as a function of fluence with the most relevant measured data from the literature, one NRC-approved industry flaw evaluation method (BWRVIP-100, Revision 1-A), and two other proposed lower bound predictions noted in the equations below [31] and the other a modified version of the original MRP-276 equation to fit the latest data). In Figure 12, the BWRVIP-100, Revision 1-A, criteria are clearly not bounding of the data from ANL [32] (i.e., from a cancelled BWR core shroud weld irradiated at Halden) or the Zorita weld data. The results from the Zorita core barrel base metal and HAZ are approximately bounded by BWRVIP-100, Revision 1-A, but the MRP-276 lower bound curve appears to be a better approach that could be modified to bound the measured data for all regions of the weld zone. The modified MRP-276 lower bound curve uses a similar formula, with updated coefficients to ensure it bounds the Zorita data. The original and modified MRP--276 equations are shown below:

Original: $K = 180 - 142 * (1 - e^{-dpa})$

Modified: $K = 130 - 92 * (1 - e^{-dpa})$

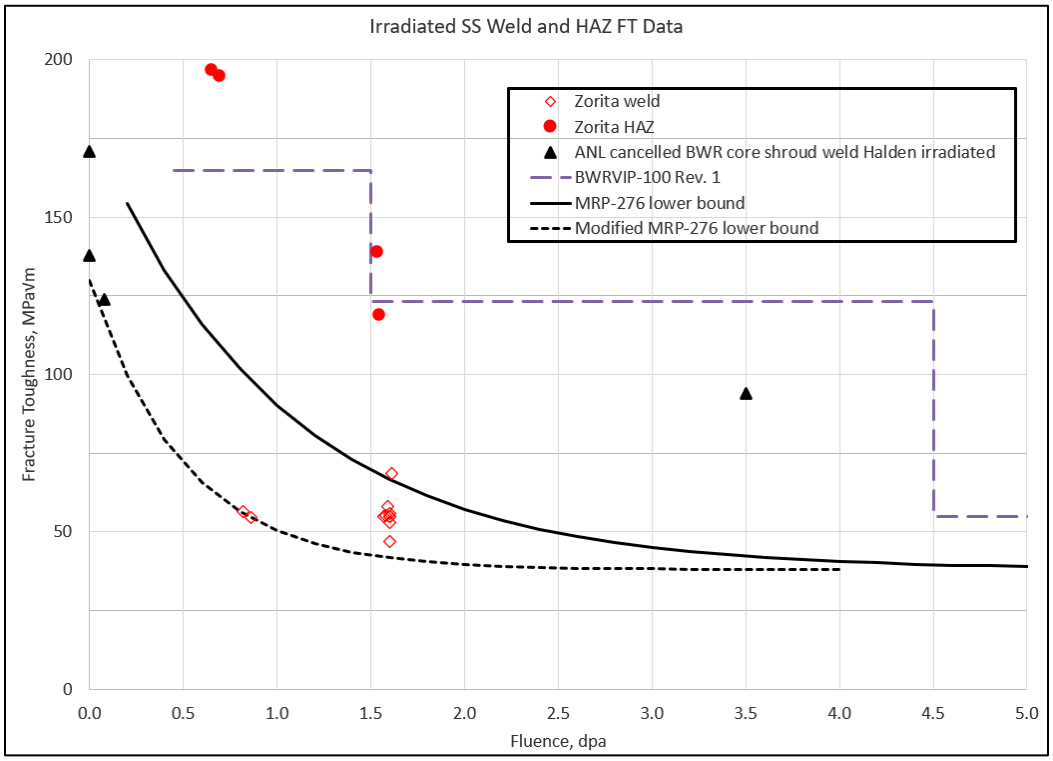

Figure 13: Summary plot of irradiated SS weld FT data as a function of fluence for Zorita and related materials

The nuclear industry makes extensive use of the guidance in BWRVIP-100, Revision 1-A, to determine inspection intervals and evaluate the significance of any flaws detected during in-service inspections of the internals. These low FT data from the Zorita materials suggest the BWRVIP-100, Revision 1-A, and WCAP–17096 guidance are sufficient for FT of irradiated base metal and HAZ, but not for the weld metal. In particular, the fluence threshold for transition from elastic-plastic fracture mechanics to linear elastic fracture mechanics may need to be reduced to appropriately bound these new data. Fortunately, as shown in Appendix B, the weld and HAZ materials from Zorita have shown strong resistance to IASCC crack growth, so there should be

less concern with large flaws growing during service into the weld metal. However, these data suggest that embrittlement of the weld metal during service could be a concern for preexisting flaws (from fabrication, for instance) or slowly growing SCC flaws under accident loading conditions if toughness were to continue decreasing at higher fluences. The NRC's LIC 504 assessment [29] indicates the low weld fracture toughness is not an immediate safety issue for BWR core shrouds, based on the operating experience related to flaws found in service and conservative loading assumptions.

Historically, the HAZ has been the region where fatigue cracking and SCC have initiated because of the local stress concentration, high residual stresses, a sensitized microstructure, and lower flow strength than the weld metal [16,33]. In the scenario of a flaw outside of the weld in the HAZ or base metal, the better resistance of the weld to SCC and the higher strength of the weld may prevent the crack in the base metal/HAZ from growing into the weld. Since the service-induced flaws tend to form in the HAZ, most cracks will tend to take the path of least resistance, away from the higher strength, more SCC-resistant, low-toughness weld metal. Under potential accident conditions in which the load is increased significantly, a flaw that was growing in the HAZ could move into the lower toughness weld metal, as demonstrated during toughness testing of HAZ material (see Figure 14), but only after significant plasticity at the crack tip.

To further explore these results, it would be beneficial to generate additional irradiated SS FT experimental data. The greatest priority would be to generate additional data at these fairly low fluence levels (<2 dpa) on harvested materials that have seen significant thermal aging as well as low-dose irradiation. Ideally, these could be compared to unirradiated thermally aged materials and as- welded properties to differentiate the effects of thermal aging and irradiation on embrittlement. Additional characterization of oxygen content and the original welding process would also be helpful in future work on harvested materials. Finally, higher fluence levels should be explored to understand FT and CGR behavior at higher dose levels that will be seen in both BWRs and PWRs during extended plant operation. The OECD/NEA SMILE project expects to test SS weld materials with up to 7 dpa of exposure from the Ringhals 2 plant, which could help address several of these data needs. Other domestic harvesting opportunities are also being pursued on higher dose SS weld materials.

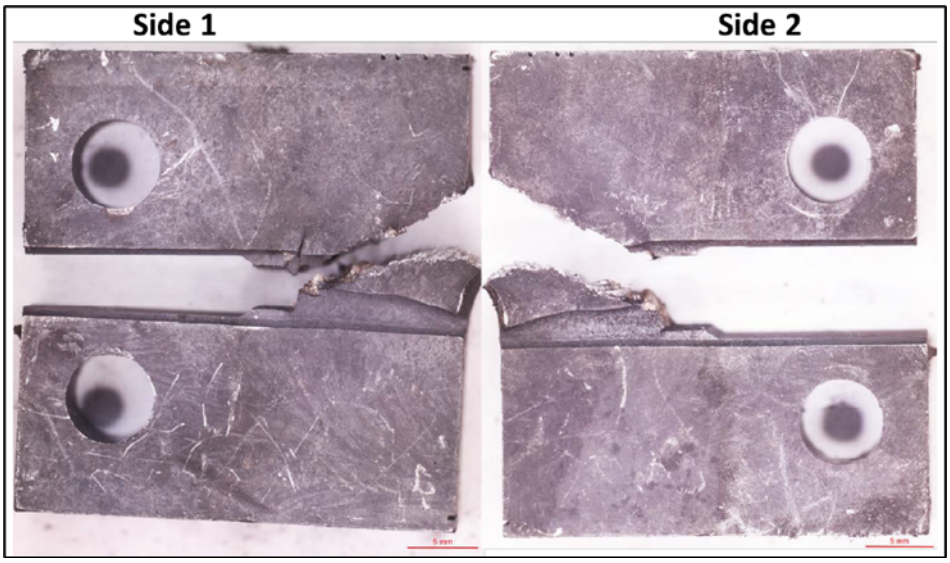

Figure 14: Side views of specimen W2HCT03 after testing, showing that the crack deviated from the plane defined by the side grooves during the FT test (Ref: Figure C-80 from MRP-451)

CHAPTER 4: CONCLUSIONS AND RECOMMENDATIONS

The Zorita materials research programs have investigated highly representative high-fluence irradiated SS components harvested from a commercial PWR. The most significant results from the testing of Zorita baffle plate materials are the repeated observations of high CGR during IASCC CGR testing and the very low amount of observed void swelling. The most significant results from the testing of Zorita weld materials are the very low FT values observed in multiple tests.

The Zorita baffle plate void swelling data should be taken as encouraging in that void swelling may not progress as rapidly in LWRs as previously suggested. However, due to the lower operating temperatures of Zorita, the results cannot conclusively eliminate the potential for significant void swelling, particularly at higher doses and temperatures. The Zorita void swelling data show the strong influence of temperature, consistent with the results from other data in the literature. Industry and regulators should seek to observe additional LWR-irradiated materials at higher doses and temperatures near 360 degrees C to more confidently conclude that void swelling will not pose a significant issue during extended operating periods.

The Zorita baffle plate CGR data suggest that the IASCC CGR model for ASME Code Case N-889 does not sufficiently predict the increased IASCC CGRs at fluences above 20 dpa observed in this material. This deficiency supports the proposed NRC condition on this Code Case, limiting its applicability to materials less than 20 dpa. Given the small volume of LWR internals exceeding 20 dpa, the practical implications of this condition are likely to be limited in the near term. When assessing the significance of the high CGRs on Zorita materials at high fluence levels, it should also be recognized that these data come from one heat of material irradiated in one reactor. Heat-to-heat variability can lead to significant uncertainty in materials testing, so additional CGR testing of highly irradiated materials should be pursued where practical to augment the Zorita plate testing data and confirm or refute the observations from the Zorita CGR testing. The SMILE project will harvest and test Type 304 SS internals materials from the Ringhals 2 PWR with fluences up to 50 dpa. The SMILE data and other future harvesting efforts should help to provide additional understanding of the IASCC behavior of high-fluence PWR internals.

The Zorita core barrel weld FT data should be carefully considered when assessing irradiated SS weld embrittlement, particularly given the very limited amount of data from in-service welds. The Zorita data should be used to update existing guidance on irradiated SS weld FT as contained in BWRVIP-100, Revision 1, and WCAP-17096. Given the low susceptibility to IASCC, low operating stresses, and flaw-tolerant design of the BWR core shroud and PWR core barrel, it is not expected that these lower weld FT data pose an immediate safety concern. However, these results may necessitate reduced inspection intervals compared to previous guidance to ensure that an acceptable margin to structural integrity exists. Further research on irradiated SS weld materials should prioritize generating additional data at fairly low fluence levels (<2 dpa) and extend data on irradiated SS weld properties up to higher fluences approaching 20–30 dpa. Further harvesting efforts planned through the SMILE program and at a domestic plant to acquire PWR-irradiated SS weld and HAZ materials at a range of fluences are expected to help address these data needs.

REFERENCES[5]

1. Electric Power Research Institute, "Materials Reliability Program: Zorita Internals Research Project (MRP-440), Testing of Highly-Irradiated Baffle Plate Material," Product ID 3002016015, Palo Alto, CA, October 29, 2019 (proprietary; available for viewing through the NRC Technical Library[6]).

2. Electric Power Research Institute, "Materials Reliability Program: Zorita Internals Research Project: Radiation and Temperature Analysis of Zorita Baffle Plate and Core Barrel Weld Material (MRP-392)," Product ID 3002003084, Palo Alto, CA, 2015 (proprietary).

3. Electric Power Research Institute, "Materials Reliability Program: Fluence Effects on Stainless Steel Welds (MRP-451): Crack Growth Rate and Fracture Toughness Testing of Zorita Weld and HAZ Materials," Product ID 3002018250, Palo Alto, CA, July 30, 2020 (proprietary; available for viewing through the NRC Technical Library[6]).

4. Karlsen, T.M., "Final Report on the BWR Crack Growth Rate Investigation IFA-791 (HWR-1236)," Halden Reactor Project, Halden, Norway, 2018 (proprietary).

5. Karlsen, T.M., "Interim Report on the PWR Crack Growth Rate Investigation IFA-817 (HWR-1320)," Halden Reactor Project, Halden, Norway, 2021 (proprietary).

6. Chen, Y., B. Alexandreanu, and K. Natesan, "Crack Growth Rate and Fracture Toughness Tests on Irradiated Ex-Plant Materials," ANL-19/45, Argonne National Laboratory, Lemont, IL, July 2020. (ADAMS Accession No. ML20198M503).

7. Chen, Y., W-Y. Chen, and B. Alexandreanu, "Irradiated Microstructure of Zorita Materials," ANL-20/50, Argonne National Laboratory, Lemont, IL, August 2020. (ADAMS Accession No. ML20269A143).

8. Kombaiah, B., C. Judge, J. Charboneau, S. Smith, L. Gimenes Rodrigues Albuquerque, and V. Montes de Oca Carioni, "Chemical Compositional Analysis and Microstructural Characterization of Harvested Zorita Reactor Pressure Vessel (RPV) Internals," INL/EXT-21-62220, Idaho National Laboratory, Idaho Falls, ID, March 2021. (ADAMS Accession No. ML21124A112)

9. Electric Power Research Institute, "BWRVIP-294, Rev. 2: Fracture Toughness of Zorita RPV Core Internals Applicable to BWRs: Final Report 2019," Product ID 3002015929, Palo Alto, CA, October 2019 (proprietary).

5. Publicly available NRC published documents are available electronically through the NRC Library on the NRC's public Web site at http://www.nrc.gov/reading-rm/doc-collections/. The documents can also be viewed online or printed for a fee in the NRC's Public Document Room (PDR) at 11555 Rockville Pike, Rockville, MD; the mailing address is USNRC PDR, Washington, DC 20555; telephone (301) 415-4737 or (800) 397-4209; fax (301) 415-3548; and e-mail pdr.resource@nrc.gov.

6. The Technical Library, which is located at Two White Flint North, 11545 Rockville Pike, Rockville, Maryland 20852, is open by appointment only. Interested parties may make appointments to examine documents by contacting the NRC Technical Library by email: Library.Resource@nrc.gov between 8:00 a.m. and 4:00 p.m. (EST), Monday through Friday, except Federal holidays.

10. Electric Power Research Institute, “BWRVIP-335: BWR Vessel and Internals Project, Crack Growth Rate Testing of Zorita Core Barrel Materials in BWR Environments,” Product ID 3002017168, Palo Alto, CA, August 2020 (proprietary).

11. Jenssen, A. J. Stjärnsäter, K. Kese, R. Carter, J. Smith, A. Demma, and M. Hiser, “Fracture Toughness Testing of an Irradiated PWR Core Barrel Weld,” Fontevraud 9—Contribution of Materials Investigations and Operating Experience to LWRs’ Safety, Performance and Reliability, Avignon, France, September 17–20, 2018.

12. Eason, E., and R. Pathania, “Irradiation-Assisted Stress Corrosion Crack Growth Rates of Austenitic Stainless Steels in Light Water Reactor Environments,” 17th International Conference on Environmental Degradation of Materials in Nuclear Power Systems—Water Reactors, Ottawa, Ontario, Canada, August 9–12, 2015.

13. Eason, E. D., and Pathania, R. “Disposition Curves for Irradiation-Assisted Stress Corrosion Cracking of Austenitic Stainless Steels in Light Water Reactor Environments,” Proc. ASME 2015 Pressure Vessels & Piping Conference, Boston MA. Paper PVP2015-45323, July 19-23, 2015.

14. Jenssen, A., J. Stjärnsäter, C. Topbasi, and P. Chou, “Specimen Size Effects on the Crack Growth Rate Response of Highly Irradiated Type 304 Stainless Steel,” 19th International Conference on Environmental Degradation of Materials in Nuclear Power Systems—Water Reactors, Boston, MA, August 18–22, 2019.

15. Electric Power Research Institute, “BWRVIP-315: BWR Vessel and Internals Project, Reactor Internals Aging Management Evaluation for Extended Operations,” Product ID 3002012535, Palo Alto, CA, July 2019 (proprietary).

16. Chopra, O.K. “Degradation of LWR Core Internal Materials due to Neutron Irradiation,” NUREG/CR-7027, ANL-10/11, Argonne National Laboratory, Lemont, IL, December 2010. (ADAMS Accession No. ML102790482)

17. Miura, T., K. Fujii, K. Fukuya, and Y. Kitsunai, “Micro-tensile testing for grain boundary fracture in neutron-irradiated stainless steels,” Materials in Nuclear Energy Systems, American Nuclear Society, Baltimore, MD, October 6–10, 2019.

18. U.S. Nuclear Regulatory Commission. Draft Regulatory Guide DG-1367 “Inservice Inspection Code Case Acceptability, ASME Section XI, Division 1,” January 2021. (ADAMS Accession No. ML20120A631).

19. Garner, F.A. Chapter 10, "Void swelling and irradiation creep in light water reactor (LWR) environments", in Understanding and Mitigating Ageing in Nuclear Power Plants, Ed. P. G. Tipping, Woodhouse Publishing, 2010, pp. 308-356.

20. Garner, F., “New data and insights on prediction of void swelling in austenitic pressure vessel internals,” Fontevraud 9—Contribution of Materials Investigations and Operating Experience to LWRs’ Safety, Performance and Reliability, Avignon, France, September 17–20, 2018.

21. Palm, N., B. Carter. “Potential Non-Conservatism in EPRI Report, BWRVIP-100, Rev. 1-A, and EPRI Software, BWRVIP-235 (Closed Session),” presentation at NRC public meeting on May 27, 2021. (ADAMS Accession No. ML21147A009).

22. Electric Power Research Institute, “BWRVIP-100NP, Revision 1-A: BWR Vessel and Internals Project, Updated Assessment of the Fracture Toughness of Irradiated Stainless Steel for BWR Core Shrouds,” Product ID 3002008388NP, Palo Alto, CA, February 2017. (ADAMS Accession No. ML17076A228)

23. Carpenter, B.T., R.G. Lott, S. Fyfitch, and A. Kulp, “Reactor Internals Acceptance Criteria Methodology and Data Requirements,” WCAP-17096-NP-A, Revision 2, Westinghouse, Cranberry Township, PA, August 2016. (ADAMS Accession No. ML16279A320)

24. Electric Power Research Institute, “MRP-227, Revision 1-A: Materials Reliability Program: Pressurized Water Reactor Internals Inspection and Evaluation Guidelines,” Product ID 3002018304, Palo Alto, CA, December 2019 (ADAMS Accession No. ML19339G350).

25. Palm, N., Hanley, T. “BWRVIP-2021-030: Potential Non-Conservatism in EPRI Report, BWRVIP-100, Rev. 1-A, 3002008388 and Impacted BWRVIP Reports,” letter dated March 22, 2021. (ADAMS Accession No. ML21084A164)

26. U.S. Nuclear Regulatory Commission. Title 10 of the Code of Federal Regulations Part 21, “Reporting of Defects and Noncompliance,” 42 FR 28893, June 6, 1977, unless otherwise noted [77 FR 39905, Jul. 6, 2012; 80 FR 54233, Sep. 9, 2015]. (https://www.nrc.gov/reading-rm/doc-collections/cfr/part021/index.html)

27. Radonovich, D.C., E.W. Deemer, R. Hosler, S. Davidsaver, G. Troyer and S. Fyfitch, “Reactor Internals Acceptance Criteria Methodology and Data Requirements,” WCAP-17096-NP, Revision 3, Westinghouse, Cranberry Township, PA, July 2019. (ADAMS Accession No. ML19218A179)

28. D. Radonovich, J.B. Hall. “PWROG Evaluation of the Potential Non- Conservative Fracture Toughness in BWRVIP-100, Rev. 1-A,” presentation at NRC public meeting on May 27, 2021. (ADAMS Accession No. ML21147A012).

29. Buford, A., “Technical Assessment of Nonconservative Fracture Toughness in Boiling Water Reactor Vessel and Internals Project Topical Report, BWRVIP-100, Revision 1-A,” November 17, 2021. (ADAMS Accession No. ML21312A543 (package))

30. U.S. Nuclear Regulatory Commission. “LIC-504, Revision 5 Integrated Risk-Informed Decisionmaking Process for Emergent Issues,” March 9, 2020. (ADAMS Accession No. ML19253D401)

31. Electric Power Research Institute, “Materials Reliability Program: Thermal Aging and Neutron Embrittlement Assessment of Cast Austenitic Stainless Steels and Stainless Steel Welds in PWR Internals (MRP-276),” Product ID 1020959, Palo Alto, CA, May 12, 2010.

32. Chen,Y., B. Alexandreanu, C. Xu, Y. Yang, K. Natesan, and A. S. Rao, “Environmentally Assisted Cracking and Fracture Toughness of an Irradiated Stainless Steel Weld,” 19th International Conference on Environmental Degradation of Materials in Nuclear Power Systems—Water Reactors, Boston, MA, August 18–22, 2019.

33. Andresen, P.L. Chapter 9, "Stress corrosion cracking (SCC) of austenitic stainless steels in high temperature light water reactor (LWR) environments", in Understanding and Mitigating Ageing in Nuclear Power Plants, Ed. P. G. Tipping, Woodhouse Publishing, 2010, pp. 236-307.

APPENDIX A: ADDITIONAL ZORITA PLATE TESTING RESULTS

A.1 Overview of Zorita Plate Testing

Zorita baffle plate testing and characterization was performed at Studsvik, Halden, Argonne National Laboratory, and Idaho National Laboratory under various programs covering tensile, irradiation-assisted stress corrosion cracking (IASCC) crack initiation, IASCC crack growth rate (CGR), fracture toughness (FT), and TEM to assess irradiation damage and void swelling.

The Zorita plate CGR and void swelling results were the most noteworthy and are discussed in detail in Section 3 of the main body of this report, while this appendix covers other results obtained during the test program, including tensile, crack initiation, and FT testing.

A.2 Plate Tensile Testing

Figure A-1, from Materials Reliability Program (MRP)-440 [1], summarizes the tensile test results compared to those from other data in the literature. The data are consistent with the general trend for irradiated stainless steels (SSs) and do not offer any significantly new insights into irradiated SS behavior.

A.3 Plate Crack Initiation Testing

Figure A-2, from MRP-440, summarizes the IASCC initiation test results on O-ring and uniaxial constant load specimens compared to those from other data in the literature. The data are in line with the general trend for irradiated SSs and tend to confirm the Electric Power Research Institute MRP trendline for IASCC initiation as a function of dose and applied stress.
One interesting aspect of the IASCC initiation data from the Zorita materials was that no O-ring specimens failed (note open blue squares in Figure A-2). This is different from literature data on O-ring samples. However, it should be noted that much of the literature data on O-ring samples used flux thimble tubes with the original surface (including oxide layer) intact, while the Zorita O-ring specimens were machined from a plate and polished. The differing product form and surface condition of the tested Zorita materials may explain the differing behavior compared to O-ring literature data.

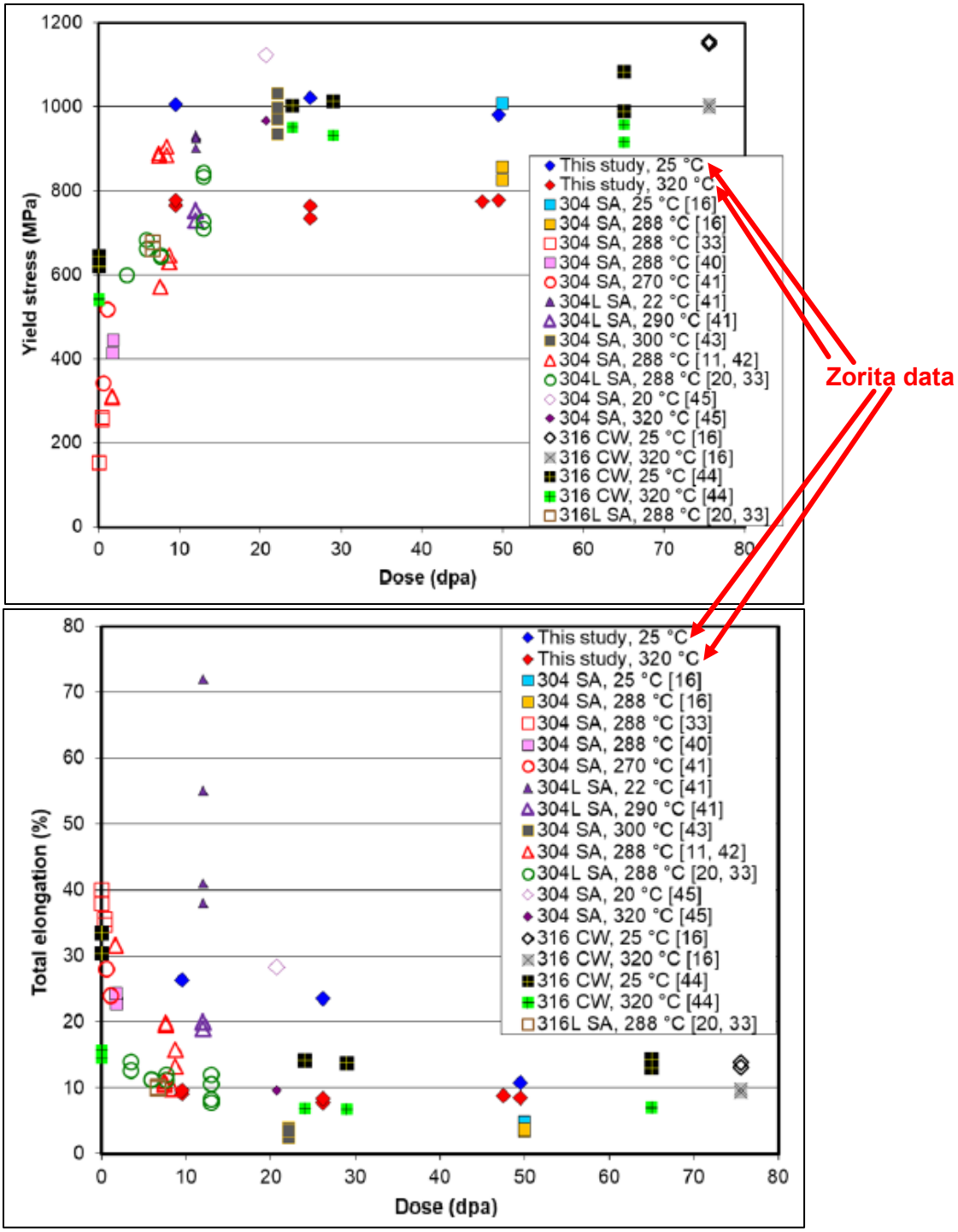

Figure A-1: Yield stress (top) and total elongation (bottom) as a function of dose (Ref: Figures 8-3 and 8-4 from MRP-440)[4]

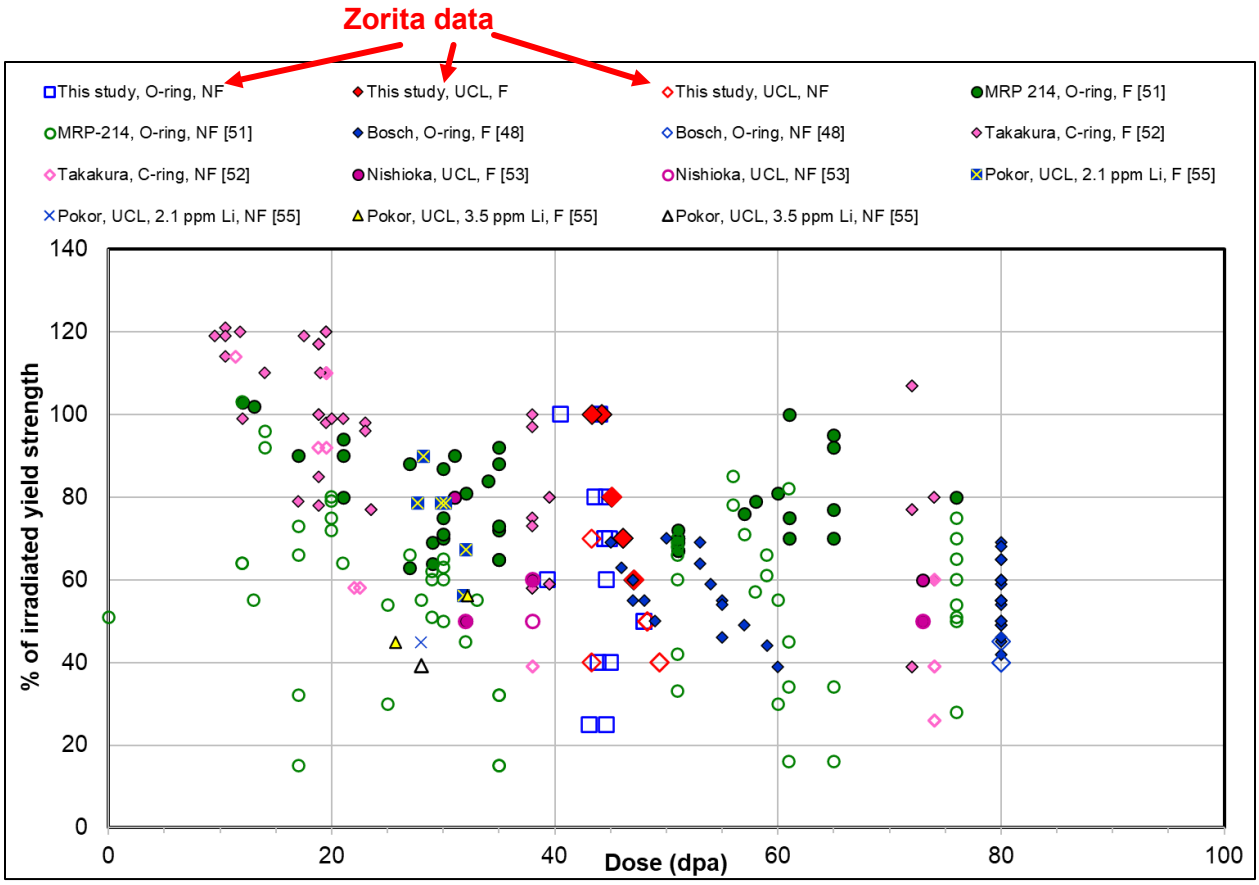

Figure A-2: Summary of IASCC crack initiation results on Zorita plate materials compared to literature data (Ref: Figure 8-6 from MRP-440)[4]

A.4 Plate Fracture Toughness Testing

Figure A-3, from MRP-440, summarizes the FT test results compared to other literature data. The data are consistent with the general trend for irradiated SSs, with the principal new insight being that FT decreases largely saturate at doses above 10 displacements per atom (dpa). This is an important finding as plants age and licensees may find flaws in components at higher doses.

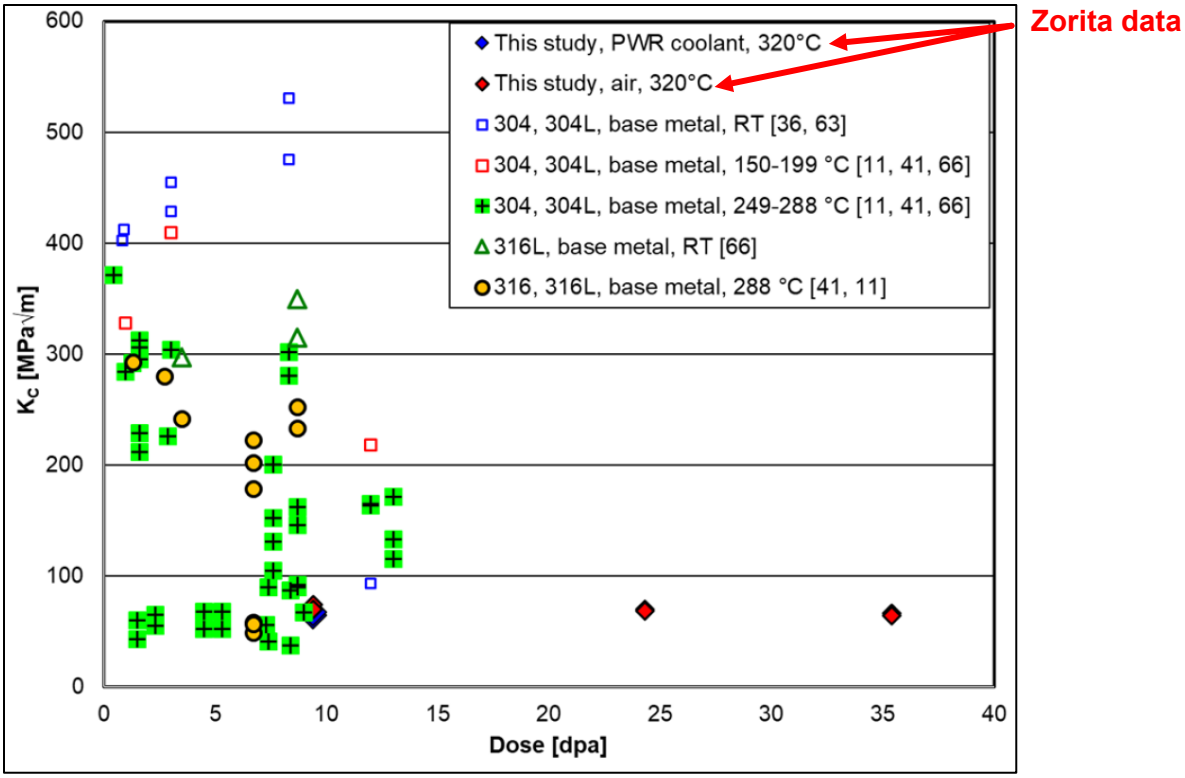

Figure A-3: Summary of FT results on Zorita plate materials compared to literature data (Ref: Figure 8-24 from MRP-440)[4]

APPENDIX B: ADDITIONAL ZORITA WELD AND HEAT-AFFECTED ZONE TESTING RESULTS

B.1 Overview of Zorita Weld and Heat-Affected Zone Testing

The goal of the testing program was to evaluate the effects of irradiation on stainless steel (SS) welds. To this end, tensile testing, microstructural characterization by light optical microscopy, fracture toughness (FT) testing, and stress corrosion crack growth rate (CGR) testing were performed on SS weld and heat-affected zone (HAZ) specimens machined from the Zorita core barrel at doses in the range of 0.7–1.9 displacements per atom (dpa). In addition to testing in air, some tests were conducted in simulated pressurized-water reactor (PWR) primary water conditions and PWR shutdown chemistry conditions at 170 degrees Celsius (C).

The Zorita weld and HAZ FT results were the most noteworthy and are discussed in detail in Section 4 of the main body of this report, while this appendix covers other results obtained during the test program, including tensile and CGR testing.

B.2 Weld and Heat-Affected Zone Tensile Testing

Figure B-1 from Materials Reliability Program (MRP)-451 [3] summarizes the tensile test results, in conjunction with literature data on irradiated SS weld/HAZ materials.

For both weld and HAZ materials, the yield stress generally follows the trend of the few other data points available in the literature. However, for ductility, both weld and HAZ materials from Zorita show significantly lower ductility compared to materials at similar doses described in the literature. This interesting observation appears to be consistent with the very low FT also observed in these materials, which is discussed in greater detail in Section 4 of the main body of this report.

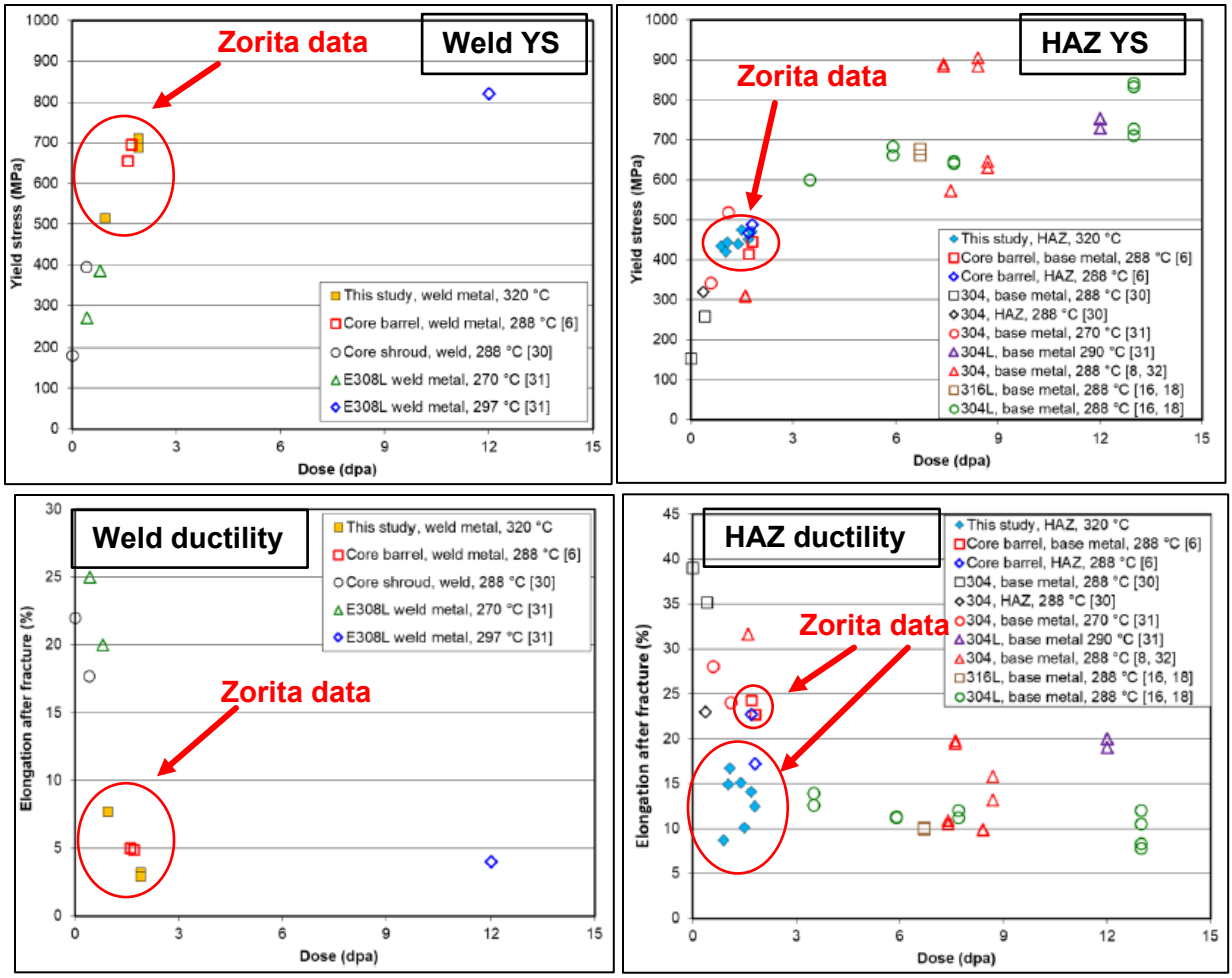

Figure B-1: Summary of tensile results: weld yield stress (top left), HAZ yield stress (top right), weld ductility (bottom left), HAZ ductility (bottom right) compared to literature data (Ref.: Figures 7-3 through 7-6 from MRP-451)[4]

B.3 Weld/Heat-Affected Zone Crack Growth Rate Testing

A fairly extensive CGR test matrix was performed on the Zorita weld and HAZ materials as shown below in Table B-1 (Ref: Table 5-1 from MRP-451).

Table B-1: Test Matrix for Crack Growth Rate Testing in PWR Primary Water

Specimen ID	Material	Dose, dpa	KI,	Test temperature, °C	Environment
W2WCT03	Weld	1.53	~30	290, 320, 340	PWR primary water*
W2WCT06	Weld	1.53	~15 and 25	290, 320, 340	
W2HCT03	HAZ	1.48	~25	290, 320, 340	
W2HCT06	HAZ	1.48	~30	290, 320, 340	
W2WCT05	Weld	1.53	~30	170	Shutdown chemistry*
W2WCT04	Weld	1.53	~30	170	

*PWR primary water simulated by the addition of 1000 ppm B, 2 ppm Li and 30 cm^3/kg of hydrogen at the temperatures indicated, and shutdown chemistry simulated by the addition of 2000 ppm B and 15 cm^3/kg of hydrogen to water at 170 ºC

Figure B-2, from MRP-451, shows the results from the CGR testing, with temperature correction and comparison to the irradiation-assisted stress corrosion cracking (IASCC) CGR model from American Society of Mechanical Engineers (ASME) Code Case N-889. The key takeaway from the weld/HAZ CGR testing is that all the weld and HAZ specimens tested in this study were very resistant to IASCC in the environments investigated, as it was very difficult to obtain sustained crack growth under constant stress intensity factor (K) conditions. All data fall well below the ASME Code Case N-889 IASCC CGR model curves, even though most of the data were obtained under loading conditions that involved partial periodic unloading and a hold time at maximum load.

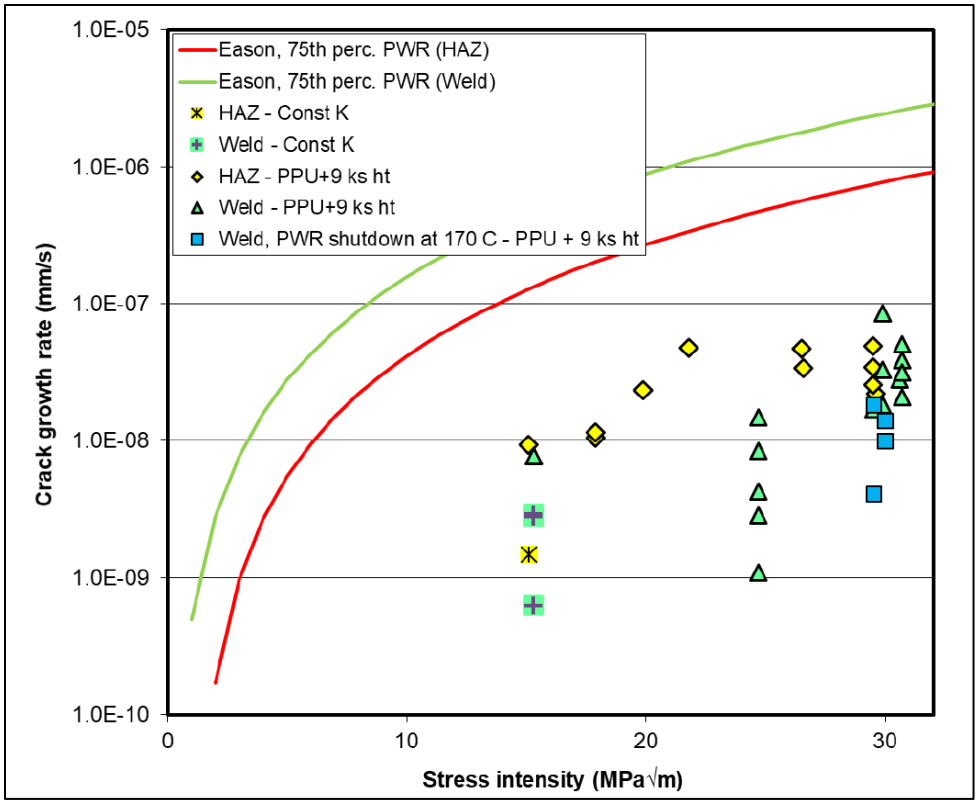

Figure B-2: Summary of constant K and partial periodic unloading (PPU) IASCC CGR data in PWR conditions normalized to 320 degrees C compared to the Eason/Electric Power Research Institute IASCC CGR model curve from ASME Code Case N-889 for this temperature/chemistry (Ref: Figure 7-8 from MRP-451)

APPENDIX C: ADDITIONAL ZORITA PLATE CGR TESTING TABULAR DATA

CGR Data from Studsvik [1]

Table C-1 Crack growth rate data for Specimen B1CT01 (41.5 dpa) based on corrected (non-linear) DCPD data

Step	R ratio	Load[1] condition	Temp.[2] ºC	CGR[3] mm/s	K_{Istart} MPa√m[4]	K_{Istop} MPa√m[4]	Δt hours[5]	Δa mm[5]	K validity, %[6]		
									399	ΔYS/2	ΔYS/3
1	0.2	1	320	$1.78 \cdot 10^{-5}$	13.0	13.1	27.5	1.089	24	39	50
2	0.6	1	320	$8.49 \cdot 10^{-6}$	16.1	16.1	2.5	0.079	30	49	62
3	0.6	0.1	320	$8.30 \cdot 10^{-7}$	16.1	16.1	35.2	0.102	30	49	62
4	0.6	0.01	320	$1.62 \cdot 10^{-7}$	16.1	16.2	265.5	0.153	30	49	62
5a	0.6	0.001	320	$3.52 \cdot 10^{-8}$	16.2	16.3	256.8	0.025	30	49	62
5b	0.6	0.001	320	$3.15 \cdot 10^{-8}$	16.3	16.3	152.4	0.017	30	49	62
6a	0.6	100 s hold	320	$2.63 \cdot 10^{-8}$	16.3	16.3	25.5	0.007	30	49	62
6b	1	Const. P	320	$1.04 \cdot 10^{-8}$	16.3	16.3	76.9	0.003	30	49	62
6c	0.6	100 s hold	320	$2.93 \cdot 10^{-8}$	16.3	16.3	238.5	0.022	30	49	62
6d	0.6	1 ks hold	320	$2.12 \cdot 10^{-8}$	16.3	16.3	163.4	0.013	30	49	62
6e	0.6	9 ks hold	320	$1.41 \cdot 10^{-8}$	16.3	16.3	144.5	0.007	30	49	62
7	1	Const. K	320	$2.56 \cdot 10^{-8}$	16.3	16.3	213.5	0.020	30	49	62
8	1	Const. K	340	$5.25 \cdot 10^{-8}$	16.3	16.4	262.5	0.048	30	49	62
9	1	Const. K	290	$2.37 \cdot 10^{-8}$	16.4	16.4	336.0	0.032	31	50	63
10a	1	Const. K	320	$1.02 \cdot 10^{-8}$	16.4	16.5	194.3	0.013	31	50	63
10b	0.6	9 ks hold	320	$9.86 \cdot 10^{-8}$	16.5	16.5	44.4	0.016	31	50	63
10c	1	Const. K	320	$1.18 \cdot 10^{-8}$	16.5	16.5	265.9	0.016	31	50	63
11	0.2	1	320	$9.26 \cdot 10^{-5}$	21.7	22.1	2.5	0.889	40	66	83
12	0.6	1	320	$2.33 \cdot 10^{-5}$	26.2	26.2	0.8	0.069	49	79	100

Table C-1 (continued) Crack growth rate data for Specimen B1CT01 (41.5 dpa) based on corrected (non-linear) DCPD data

Step	R ratio	Load[1] condition	Temp.[2] ºC	CGR[3] mm/s	K_{Istart} MPa$\sqrt{m}$[4]	K_{Istop} MPa$\sqrt{m}$[4]	Δt hours[5]	Δa mm[5]	K validity, %[6]		
									399	ΔYS/2	ΔYS/3
13	0.6	0.1	320	$3.08 \cdot 10^{-6}$	26.2	26.2	9.2	0.101	49	79	100
14	0.6	0.01	320	$2.60 \cdot 10^{-7}$	26.2	26.2	113.6	0.108	49	79	100
15	0.6	0.001	320	$3.38 \cdot 10^{-8}$	26.2	26.3	185.1	0.026	49	79	100
16a	0.6	100 s hold	320	$3.95 \cdot 10^{-8}$	26.3	26.3	170.9	0.022	49	79	100
16b	0.6	1 ks hold	320	$2.81 \cdot 10^{-8}$	26.3	26.3	164.2	0.020	49	79	100
16c	0.6	9 ks hold	320	$1.49 \cdot 10^{-8}$	26.3	26.3	197.3	0.012	49	80	100
17a	1	Const. K	320	$1.07 \cdot 10^{-6}$	26.3	26.5	29.8	0.114	49	80	101
17a1	1	Const. K	320	$3.33 \cdot 10^{-7}$	26.3	26.3	14.5	0.015	49	80	101
17a2	1	Const. K	320	$1.67 \cdot 10^{-6}$	26.3	26.5	15.3	0.099	49	80	101
17b	1	Const. K	320	$1.17 \cdot 10^{-5}$	26.5	27.3	10.8	0.468	49	80	101
17b1	1	Const. K	320	$7.56 \cdot 10^{-6}$	26.5	26.8	6.3	0.173	49	80	101
17b2	1	Const. K	320	$1.90 \cdot 10^{-5}$	26.8	27.3	4.5	0.295	50	81	103
18	1	dK/da=-	320	$1.46 \cdot 10^{-5}$	27.3	22.9	12.0	0.603	52	84	106
19	1	dK/da=-	320	$1.10 \cdot 10^{-5}$	22.9	21.1	6.7	0.258	45	72	91
20	1	Const. K	320	$2.97 \cdot 10^{-5}$	21.1	23.1	9.5	0.963	42	68	85
21a	1	dK/da=-	320	$2.99 \cdot 10^{-5}$	23.1	21.3	2.4	0.259	48	77	98
21b	1	dK/da=-	320	$1.27 \cdot 10^{-5}$	20.3	18.9	3.9	0.179	43	70	88
21c	1	dK/da=-	320	$4.54 \cdot 10^{-6}$	18.7	17.9	5.9	0.098	40	65	82
21d	1	dK/da=-	320	$2.26 \cdot 10^{-8}$	17.7	17.7	95.1	0.007	38	62	78
22	1	Const. K	320	$1.73 \cdot 10^{-8}$	17.7	17.7	120.3	0.007	38	62	78
23a[7]	0.6	dK/da=+4.7	320	$4.59 \cdot 10^{-6}$	17.7	20.4	16.5	0.326	38	62	78

Table C-1 (continued) Crack growth rate data for Specimen B1CT01 (41.5 dpa) based on corrected (non-linear) DCPD data

Step	R ratio	Load[1] condition	Temp.[2] ºC	CGR[3] mm/s	K_{Istart} MPa√m[4]	K_{Istop} MPa√m[4]	Δt hours[5]	Δa mm[5]	K validity, %[6]		
									399	ΔYS/2	ΔYS/3
23b[7]	0.6	dK/da=+4.7	320	$4.31 \cdot 10^{-4}$	20.4	25.1	0.5	0.714	45	73	92
24a	1	dK/da=+5	320	$1.14 \cdot 10^{-6}$	25.1	26.9	36.8	0.256	58	94	119
24b	1	dK/da=+5	320	$1.41 \cdot 10^{-6}$	26.9	30.8	32.7	0.546	63	103	130
25	1	Const. K	320	$1.61 \cdot 10^{-7}$	30.8	31.3	245.5	0.154	75	122	154
26	1	Const. K	340	$2.39 \cdot 10^{-7}$	31.3	32.5	185.9	0.220	77	126	158
27	1	Const. K	290	$2.55 \cdot 10^{-5}$	32.5	137.4	22.5	4.166	82	132	167
28	1	Const. P	290	$5.19 \cdot 10^{-6}$	3.6	3.6	24.5	0.371	15	24	30

1) Loading condition during testing. A number stands for the frequency in Hz during continuous cyclic load, whereas a number followed by a time and the word “hold” means the specimen was subjected to partial periodic unloading (PPU) with the hold time at maximum load indicated. Const. K or P means testing was conducted under constant stress intensity factor (K), or load (P), while ”dK/da=X” means K was changed by the nominal rate (in MPa√m/mm) indicated.
2) Test temperature during the step.
3) Crack growth rate determined by linear regression of the corrected DCPD curve.
4) Stress intensity factor based on the crack length corresponding to the first (K_{Istart}) and last (K_{Istop}) data point of the regression analysis and load data.
5) Difference in test time or crack length between the first and last data point of the regression analysis.
6) K validity according to ASTM E399 and modified criteria based on the same standard. An effective yield strength was used for the modified criteria, i.e., $YS_{eff1}=YS_{unirr} + (YS_{irr}-YS_{unirr})/2$ and $YS_{eff2}=YS_{unirr} + (YS_{irr}-YS_{unirr})/3$. The actual K during the step was related to the K limit based on the crack length when the step started, i.e., 100% or higher means the criterion was exceeded.
7) Positive dK/da as indicated plus continuous cycling at frequency and R ratio reported.

Table C-2 Crack growth rate data for Specimen B1CT03 (41.5 dpa) based on corrected (non-linear) DCPD data

Step	R ratio	Load[1] condition	Temp.[2] °C	CGR[3] mm/s	K_{Istart} MPa√m[4]	K_{Istop} MPa√m[4]	Δt hours[5]	Δa mm[5]	K validity, %[6]		
									399	ΔYS/2	ΔYS/3
1	0.2	1	320	$3.29\cdot10^{-5}$	16.0	16.1	10.8	1.077	30	49	61
2	0.6	1	320	$1.48\cdot10^{-5}$	20.1	20.1	4.2	0.228	38	61	77
3	0.6	0.1	320	$1.93\cdot10^{-6}$	20.1	20.1	21.2	0.148	37	61	77
4	0.6	0.01	320	$2.16\cdot10^{-7}$	20.1	20.1	148.3	0.118	37	61	77
5	0.6	0.001	320	$4.13\cdot10^{-8}$	20.1	20.1	485.2	0.074	38	61	77
6a	0.6	100 s hold	320	$3.97\cdot10^{-8}$	20.1	20.2	365.7	0.048	38	61	77
6b	0.6	1 ks hold	320	$3.32\cdot10^{-8}$	20.2	20.2	353.3	0.045	38	61	77
6c	0.6	9 ks hold	320	$2.72\cdot10^{-8}$	20.2	20.2	258.5	0.027	38	61	77
6d	0.6	9 ks hold	320	$3.11\cdot10^{-8}$	20.2	20.3	461.2	0.057	38	61	77
7a	1	Const. K	320	$1.09\cdot10^{-8}$	20.3	20.1	135.5	0.005	38	61	77
7b	1	Const. K	320	$7.22\cdot10^{-7}$	20.1	20.1	2.3	0.006	37	61	77
7c	1	Const. K	320	$7.61\cdot10^{-9}$	20.1	20.3	101.3	0.004	37	61	77
7d	0.6	9 ks hold	320	$6.09\cdot10^{-8}$	20.3	20.3	67.7	0.014	38	61	78
7e	1	Const. K	320	$1.30\cdot10^{-8}$	20.3	20.3	197.1	0.007	38	61	78
8	1	Const. K	340	$3.17\cdot10^{-8}$	20.3	20.4	333.8	0.036	38	62	78
9a	1	Const. K	290	$2.92\cdot10^{-9}$	20.4	20.4	19.9	0.001	38	62	78
9b	1	Const. K	290	$2.60\cdot10^{-5}$	23.6	27.3	17.5	1.547	44	72	90
9c	1	Const. P	290	$8.91\cdot10^{-7}$	14.1	14.2	21.6	0.069	27	44	55
9d	1	Const. P	290	$<1\cdot10^{-9}$	4.9	1.9	260.6	0.000	9	15	19
10	1	Const. K	290	$2.05\cdot10^{-5}$	22.7	27.3	28.3	1.978	43	70	89
11	1	dK/da=-16.7	290	$1.02\cdot10^{-5}$	27.4	22.2	18.7	0.691	57	93	118
12	1	Const. K	290	$3.05\cdot10^{-5}$	22.2	26.3	10.5	1.212	48	79	99

Table C-2 (continued) Crack growth rate data for Specimen B1CT03 (41.5 dpa) based on corrected (non-linear) DCPD data

Step	R ratio	Load[1] condition	Temp.[2] ºC	CGR[3] mm/s	K_{Istart} MPa√m[4]	K_{Istop} MPa√m[4]	Δt hours[5]	Δa mm[5]	K validity, %[6]		
									399	ΔYS/2	ΔYS/3
13	1	dK/da=-	290	$7.87 \cdot 10^{-6}$	26.3	23.1	10.0	0.271	62	100	126
14	1	Const. K	290	$5.11 \cdot 10^{-5}$	23.1	31.0	7.2	1.148	56	92	116
15a	1	dK/da=-	290	$4.74 \cdot 10^{-6}$	31.0	27.7	15.5	0.269	83	135	170
15b	1	dK/da=-	290	$2.48 \cdot 10^{-8}$	27.3	27.4	46.9	0.005	75	122	154
16	1	Const. K	290	$1.80 \cdot 10^{-8}$	27.4	27.2	341.4	0.021	75	122	154
17	0.6	9 ks hold	290	$3.91 \cdot 10^{-6}$	27.2	30.8	30.4	0.509	75	122	154
18	1	Const. K	290	$1.81 \cdot 10^{-8}$	30.8	30.8	133.0	0.012	89	145	183
19	1	Const. K	340	$1.63 \cdot 10^{-8}$	30.8	31.0	379.1	0.022	89	145	183
20	1	Const. K	320	$2.91 \cdot 10^{-8}$	31.0	31.0	12.4	0.002	90	146	184
21	1	Const. P	320	$<1 \cdot 10^{-9}$	4.6	4.6	72.9	0.000	13	22	28
22	0.6	9 ks hold	320	$3.63 \cdot 10^{-6}$	31.8	34.4	25.0	0.374	93	150	190
23	1	Const. K	320	$1.64 \cdot 10^{-8}$	34.4	34.7	435.0	0.028	104	169	214
24	1	Const. K	340	$3.28 \cdot 10^{-8}$	34.7	35.5	582.6	0.065	105	171	216
25	1	Const. K	340	$1.90 \cdot 10^{-5}$	35.5	60.7	23.3	1.494	108	176	222
26	1	Const. K	340	$8.35 \cdot 10^{-7}$	60.7	81.8	178.5	0.576	228	370	467

1) Loading condition during testing. A number stands for the frequency in Hz during continuous cyclic load, whereas a number followed by a time and the word “hold” means the specimen was subjected to partial periodic unloading (PPU) with the hold time at maximum load indicated. Const. K or P means testing was conducted under constant stress intensity factor (K), or load (P), while ”dK/da=X” means K was changed by the nominal rate (in MPa√m/mm) indicated.
2) Test temperature during the step.
3) Crack growth rate determined by linear regression of the corrected DCPD curve.
4) Stress intensity factor based on the crack length corresponding to the first (K_{Istart}) and last (K_{Istop}) data point of the regression analysis and load data.
5) Difference in test time or crack length between the first and last data point of the regression analysis.
6) K validity according to ASTM E399 and modified criteria based on the same standard. An effective yield strength was used for the modified criteria, i.e., $YS_{eff1}=YS_{unirr} + (YS_{irr}-YS_{unirr})/2$ and $YS_{eff2}=YS_{unirr} + (YS_{irr}-YS_{unirr})/3$. The actual K during the step was related to the K limit based on the crack length when the step started, i.e., 100% or higher means the criterion was exceeded.

Table C-3 Crack growth rate data for Specimen B2CT01 (23.9 dpa) based on corrected (non-linear) DCPD data

Step	R ratio	Load[1] condition	Temp.[2] ºC	CGR[3] mm/s	K_{Istart} MPa$\sqrt{m}$[4]	K_{Istop} MPa$\sqrt{m}$[4]	Δt hours[5]	Δa mm[5]	K validity, %[6]		
									399	ΔYS/2	ΔYS/3
1a	0.2	0.9	320	$1.08 \cdot 10^{-5}$	12.9	12.9	22.8	0.849	24	39	49
1b	0.2	0.9	320	$9.00 \cdot 10^{-6}$	12.9	12.9	4.6	0.164	24	39	49
2	0.6	0.9	320	$7.38 \cdot 10^{-6}$	16.0	16.0	3.3	0.087	30	49	61
3	0.6	0.1	320	$9.81 \cdot 10^{-7}$	16.0	16.0	28.7	0.102	30	49	61
4	0.6	0.01	320	$1.56 \cdot 10^{-7}$	16.0	16.0	176.3	0.099	30	49	61
5	0.6	0.001	320	$3.40 \cdot 10^{-8}$	16.0	16.0	320.8	0.043	30	49	61
6a	0.6	100 s hold	320	$3.70 \cdot 10^{-8}$	16.0	16.0	264.2	0.036	30	48	61
6b	0.6	1 ks hold	320	$3.10 \cdot 10^{-8}$	16.0	16.0	143.8	0.013	30	48	61
6c	0.6	9 ks hold	320	$2.27 \cdot 10^{-8}$	16.0	16.1	195.0	0.018	30	49	61
7	1	Const. K	320	$4.98 \cdot 10^{-8}$	16.1	16.1	324.4	0.050	30	49	61
8	1	Const. K	340	$6.20 \cdot 10^{-8}$	16.1	16.1	503.3	0.119	30	49	61
9	1	Const. K	290	$4.60 \cdot 10^{-8}$	16.1	16.2	837.8	0.134	30	49	62
9a	1	Const. K	290	$4.61 \cdot 10^{-8}$	16.1	16.1	573.5	0.088	30	49	62
9b	0.6	9 ks hold	290	$2.56 \cdot 10^{-7}$	16.2	16.2	24.7	0.028	30	49	62
9c	1	Const. K	290	$1.10 \cdot 10^{-8}$	16.2	16.2	239.2	0.020	30	49	62
10	1	Const. K	320	$2.08 \cdot 10^{-8}$	16.2	16.2	189.9	0.007	30	49	62
11	0.2	0.9	320	$1.12 \cdot 10^{-4}$	21.2	21.4	1.5	0.722	40	64	81
12	0.6	0.9	320	$1.84 \cdot 10^{-5}$	25.8	25.8	0.8	0.058	48	78	99
13	0.6	0.1	320	$2.12 \cdot 10^{-6}$	25.8	25.8	11.5	0.089	48	78	99
14	0.6	0.01	320	$2.38 \cdot 10^{-7}$	25.8	25.8	34.6	0.031	48	78	99

Table C-3 (continued) Crack growth rate data for Specimen B2CT01 (23.9 dpa) based on corrected (non-linear) DCPD data

Step	R ratio	Load[1] condition	Temp.[2] ºC	CGR[3] mm/s	K_{Istart} MPa√m[4]	K_{Istop} MPa√m[4]	Δt hours[5]	Δa mm[5]	K validity, %[6]		
									399	ΔYS/2	ΔYS/3
15	0.6	0.001	320	$5.50\cdot10^{-8}$	25.8	25.8	138.9	0.019	48	78	98
16	0.6	9 ks hold	320	$1.40\cdot10^{-8}$	25.8	25.8	150.0	0.016	48	78	99
17	0.6	0.001	320	$3.37\cdot10^{-8}$	25.8	25.8	89.9	0.012	48	78	99
18	0.6	0.01	320	$2.82\cdot10^{-7}$	25.8	25.8	48.1	0.047	48	78	98
19	0.6	0.001	320	$4.66\cdot10^{-8}$	25.8	25.8	340.0	0.055	48	78	99
20	0.6	100 s hold	320	$6.41\cdot10^{-8}$	25.8	25.8	168.8	0.039	48	78	99
21	0.6	1 ks hold	320	$3.74\cdot10^{-8}$	25.8	25.9	170.9	0.029	48	78	99
22	0.6	9 ks hold	320	$2.37\cdot10^{-8}$	25.9	25.9	359.1	0.031	48	78	99
23	1	Const. K	320	$<1\cdot10^{-9}$	25.9	25.9	192.6	0.000	48	78	99
24	0.4	9 ks hold	320	$5.93\cdot10^{-8}$	25.9	25.9	381.5	0.083	48	78	99
25	0.5	9 ks hold	320	$1.99\cdot10^{-8}$	25.9	26.0	336.2	0.036	48	78	99
26	0.55	9 ks hold	320	$<1\cdot10^{-9}$	26.0	26.0	334.4	0.008	48	79	99
27	0.40	1 ks hold	320	$5.73\cdot10^{-7}$	26.0	26.2	86.0	0.167	49	79	99
28	0.50	1 ks hold	320	$1.84\cdot10^{-7}$	26.2	26.3	145.1	0.102	49	79	100
29	0.60	1 ks hold	320	$5.99\cdot10^{-8}$	26.3	26.3	148.3	0.023	49	80	101
30	0.60	9 ks hold	320	$5.08\cdot10^{-8}$	26.3	26.3	94.4	0.016	49	80	101
31	1	Const. K	320	$<1\cdot10^{-9}$	26.3	26.4	265.2	0.000	49	80	101
32	0.6	9 ks hold	320	$<1\cdot10^{-9}$	26.4	26.3	310.7	0.008	49	80	101
33	0.4	0.001	320	$1.05\cdot10^{-6}$	26.3	26.5	38.1	0.155	49	80	101
34	0.5	0.001	320	$4.41\cdot10^{-7}$	26.5	26.6	33.8	0.088	50	81	102

Table C-3 (continued) Crack growth rate data for Specimen B2CT01 (23.9 dpa) based on corrected (non-linear) DCPD data

Step	R ratio	Load[1] condition	Temp.[2] ºC	CGR[3] mm/s	K_{Istart} MPa$\sqrt{m}$[4]	K_{Istop} MPa$\sqrt{m}$[4]	Δt hours[5]	Δa mm[5]	K validity, %[6]		
									399	ΔYS/2	ΔYS/3
35	0.6	0.001	320	$2.52\cdot10^{-8}$	26.6	26.7	124.2	0.006	50	82	103
36	0.5	0.001	320	$1.65\cdot10^{-7}$	26.7	26.8	116.4	0.091	50	82	103
37	0.55	0.001	320	$1.46E^{-7}$	26.8	26.9	172.2	0.083	51	82	104
38	0.6	0.001	320	$<1\cdot10^{-9}$	26.9	26.9	186.9	0.000	51	83	105
39	0.4	0.001	320	$2.10\cdot10^{-7}$	26.9	27.1	158.0	0.129	51	83	105
40	0.5	0.001	320	$1.13\cdot10^{-7}$	27.1	27.4	358.3	0.139	52	84	106
41	0.5	100 s hold	320	$4.47\cdot10^{-8}$	27.4	27.4	200.3	0.042	53	86	108
42	0.4	0.001	320	$4.86\cdot10^{-8}$	27.4	27.4	93.6	0.005	53	86	108
43	0.4	0.1	320	$2.11\cdot10^{-5}$	27.4	27.9	4.7	0.347	53	86	109
44	0.4	0.01	320	$1.32\cdot10^{-6}$	27.9	28.0	14.5	0.070	55	89	112
45	0.4	0.001	320	$1.91\cdot10^{-8}$	28.0	28.1	106.4	0.013	55	90	113
46	0.4	0.01	320	$9.81\cdot10^{-7}$	28.1	28.4	49.8	0.173	55	90	113
47	0.4	0.003	320	$2.40\cdot10^{-7}$	28.4	28.5	66.1	0.048	56	92	116
48	0.4	0.001	320	$7.46\cdot10^{-8}$	28.5	28.6	97.4	0.030	57	92	116
49	0.4	100 s hold	320	$1.02\cdot10^{-7}$	28.6	28.6	121.9	0.046	57	92	117
50	0.4	1 ks hold	320	$2.83\cdot10^{-8}$	28.6	28.6	211.8	0.027	57	93	117
51	0.4	9 ks hold	320	$<1\cdot10^{-9}$	28.6	28.7	99.9	0.000	57	93	117
52	0.3	9 ks hold	320	$3.85\cdot10^{-8}$	28.7	28.8	147.2	0.018	57	93	118
53	0.3	27 ks hold	320	$1.28\cdot10^{-8}$	28.8	28.8	195.3	0.008	58	93	118
54a	1	Const. K	320	$6.86\cdot10^{-8}$	28.8	28.8	82.6	0.018	58	94	118

Table C-3 (continued) Crack growth rate data for Specimen B2CT01 (23.9 dpa) based on corrected (non-linear) DCPD data

Step	R ratio	Load[1] condition	Temp.[2] ºC	CGR[3] mm/s	K_{Istart} MPa√m[4]	K_{Istop} MPa√m[4]	Δt hours[5]	Δa mm[5]	K validity, %[6]		
									399	ΔYS/2	ΔYS/3
54b1	1	Const. K	320	-	28.8	28.8	17.5	0.000	58	94	118
54b2	1	Const. K	320	$2.87 \cdot 10^{-6}$	28.8	29.3	10.0	0.105	58	94	118
54b3	1	Const. K	320	$1.59 \cdot 10^{-5}$	29.3	29.9	5.0	0.275	59	96	121
54b4	1	Const. K	320	$4.34 \cdot 10^{-5}$	29.9	33.4	7.0	1.082	61	99	125
54c	1	Const. P	320	$5.11 \cdot 10^{-8}$	0.7	1.6	172.0	0.039	1	2	3

1) Loading condition during testing. A number stands for the frequency in Hz during continuous cyclic load, whereas a number followed by a time and the word "hold" means the specimen was subjected to partial periodic unloading (PPU) with the hold time at maximum load indicated. Const. K or P means testing was conducted under constant stress intensity factor (K), or load (P), while "dK/da=X" means K was changed by the nominal rate (in MPa√m/mm) indicated.
2) Test temperature during the step.
3) Crack growth rate determined by linear regression of the corrected DCPD curve.
4) Stress intensity factor based on the crack length corresponding to the first (K_{Istart}) and last (K_{Istop}) data point of the regression analysis and load data.
5) Difference in test time or crack length between the first and last data point of the regression analysis.
6) K validity according to ASTM E399 and modified criteria based on the same standard. An effective yield strength was used for the modified criteria, i.e., $YS_{eff1}=YS_{unirr} + (YS_{irr}-YS_{unirr})/2$ and $YS_{eff2}=YS_{unirr} + (YS_{irr}-YS_{unirr})/3$. The actual K during the step was related to the K limit based on the crack length when the step started, i.e., 100% or higher means the criterion was exceeded.

Table C-4 Crack growth rate data for Specimen B2CT03 (23.9 dpa) based on corrected (non-linear) DCPD data

Step	R ratio	Load[1] condition	Temp.[2] ºC	CGR[3] mm/s	K_{Istart} MPa√m[4]	K_{Istop} MPa√m[4]	Δt hours[5]	Δa mm[5]	K validity, %[6]		
									399	ΔYS/2	ΔYS/3
1	0.2	1	320	$3.08 \cdot 10^{-5}$	16.1	16.1	11.5	1.058	30	49	62
2	0.6	1	320	$9.83 \cdot 10^{-6}$	20.1	20.1	6.0	0.221	38	61	77
3	0.6	0.1	320	$1.38 \cdot 10^{-6}$	20.1	20.0	31.0	0.149	37	61	77
4	0.6	0.01	320	$2.05 \cdot 10^{-7}$	20.0	20.1	158.5	0.117	37	61	77
5	0.6	0.001	320	$4.93 \cdot 10^{-8}$	20.1	20.1	273.9	0.046	38	61	77
6a	0.6	100 s hold	320	$4.40 \cdot 10^{-8}$	20.1	20.1	260.6	0.039	38	61	77
6b	0.6	1 ks hold	320	$4.21 \cdot 10^{-8}$	20.1	20.1	240.8	0.055	38	61	77
6c	0.6	9 ks hold	320	$2.78 \cdot 10^{-8}$	20.1	20.1	191.8	0.019	38	61	77
7	1	Const. K	320	$5.18 \cdot 10^{-8}$	20.1	20.2	481.0	0.072	38	61	77
7a	1	Const. K	320	$1.36 \cdot 10^{-8}$	20.1	20.1	165.6	0.008	38	61	77
7b	1	Const. K	320	$4.02 \cdot 10^{-7}$	20.1	20.1	4.2	0.004	38	61	77
7c	1	Const. K	320	$1.30 \cdot 10^{-8}$	20.1	20.2	71.0	0.004	38	61	77
7d	1	Const. K	320	$7.02 \cdot 10^{-7}$	20.2	20.2	12.5	0.035	38	61	77
7e	1	Const. K	320	$1.75 \cdot 10^{-8}$	20.2	20.2	221.8	0.016	38	61	77
8	1	Const. K	340	$4.53 \cdot 10^{-8}$	20.2	20.2	352.6	0.053	38	61	77
9a	1	Const. K	290	$5.21 \cdot 10^{-9}$	20.2	20.3	102.2	0.008	38	61	78
9b	1	Const. K	290	$2.19 \cdot 10^{-5}$	20.4	23.6	27.8	2.081	38	62	78
10a	1	Const. K	320	$4.45 \cdot 10^{-5}$	23.6	37.6	23.9	3.799	46	75	95
10a1	1	Const. K	320	$3.01 \cdot 10^{-5}$	23.6	25.9	8.9	0.992	46	75	95
10b	1	dK/da=-16.7	320	$2.79 \cdot 10^{-5}$	37.6	35.6	2.7	0.298	91	148	187

Table C-4 (continued) Crack growth rate data for Specimen B2CT03 (23.9 dpa) based on corrected (non-linear) DCPD data

Step	R ratio	Load[1] condition	Temp.[2] °C	CGR[3] mm/s	K_{Istart} MPa√m[4]	K_{Istop} MPa√m[4]	Δt hours[5]	Δa mm[5]	K validity, %[6]		
									399	ΔYS/2	ΔYS/3
10c	1	Const. K	320	$7.56 \cdot 10^{-5}$	35.6	40.8	2.0	0.536	88	143	181
10d	1	dK/da=-16.7	320	$1.94 \cdot 10^{-5}$	40.8	37.2	4.5	0.301	105	171	216
10e	1	Const. K	320	$6.27 \cdot 10^{-5}$	37.2	42.2	2.3	0.536	99	160	202
10f	1	dK/da=-16.7	320	$1.48 \cdot 10^{-5}$	42.2	39.5	5.4	0.309	117	190	240
10g	1	Const. K	320	$6.53 \cdot 10^{-5}$	39.5	46.0	2.3	0.561	113	183	231
10h	1	dK/da=-16.7	320	$5.23 \cdot 10^{-6}$	46.0	43.0	14.5	0.293	140	226	286
10k	1	Const. K	320	$2.46 \cdot 10^{-7}$	43.0	43.1	11.9	0.012	135	219	276

1) Loading condition during testing. A number stands for the frequency in Hz during continuous cyclic load, whereas a number followed by a time and the word "hold" means the specimen was subjected to partial periodic unloading (PPU) with the hold time at maximum load indicated. Const. K or P means testing was conducted under constant stress intensity factor (K), or load (P), while "dK/da=X" means K was changed by the nominal rate (in MPa√m/mm) indicated.
2) Test temperature during the step.
3) Crack growth rate determined by linear regression of the corrected DCPD curve.
4) Stress intensity factor based on the crack length corresponding to the first (K_{Istart}) and last (K_{Istop}) data point of the regression analysis and load data.
5) Difference in test time or crack length between the first and last data point of the regression analysis.
6) K validity according to ASTM E399 and modified criteria based on the same standard. An effective yield strength was used for the modified criteria, i.e., $YS_{eff1}=YS_{unirr} + (YS_{irr}-YS_{unirr})/2$ and $YS_{eff2}=YS_{unirr} + (YS_{irr}-YS_{unirr})/3$. The actual K during the step was related to the K limit based on the crack length when the step started, i.e., 100% or higher means the criterion was exceeded.

Table C-5 Crack growth rate data for Specimen B3CT03 (9.4 dpa) based on corrected (non-linear) DCPD data

Step	R ratio	Load[1] condition	Temp.[2] ºC	CGR[3] mm/s	K_{Istart} MPa$\sqrt{m}$[4]	K_{Istop} MPa$\sqrt{m}$[4]	Δt hours[5]	Δa mm[5]	K validity, %[6]		
									399	ΔYS/2	ΔYS/3
1	0.2	1	320	$1.29\cdot10^{-5}$	13.0	13.1	26.3	1.075	24	40	50
2	0.4	1	320	$2.63\cdot10^{-5}$	16.2	16.1	0.9	0.084	30	49	62
3	0.4	0.3	320	$6.52\cdot10^{-6}$	16.1	16.1	2.1	0.050	30	49	62
4	0.4	0.1	320	$2.27\cdot10^{-6}$	16.1	16.1	6.5	0.051	30	49	62
5	0.4	0.03	320	$7.94\cdot10^{-7}$	16.1	16.1	17.3	0.050	30	49	62
6	0.4	0.01	320	$3.31\cdot10^{-7}$	16.1	16.1	51.2	0.059	30	49	62
7	0.4	0.003	320	$1.14\cdot10^{-7}$	16.1	16.1	138.7	0.061	30	49	62
8	0.4	0.001	320	$5.17\cdot10^{-8}$	16.1	16.1	303.3	0.052	30	49	62
9	0.5	0.001	320	$4.45\cdot10^{-8}$	16.1	16.2	362.4	0.061	30	49	62
10	0.6	0.001	320	$2.66\cdot10^{-8}$	16.2	16.2	359.9	0.036	30	49	62
11a	0.6	100 s hold	320	$2.14\cdot10^{-8}$	16.2	16.2	137.3	0.012	30	49	62
11b	0.6	100 s hold	320	$2.42\cdot10^{-8}$	16.2	16.2	185.0	0.016	30	49	62
12	0.6	1 ks hold	320	$1.56\cdot10^{-8}$	16.2	16.2	215.6	0.013	30	49	62
13	0.6	9 ks hold	320	$7.17\cdot10^{-9}$	16.2	16.2	289.0	0.004	30	49	62
14	1	Const. K	320	$2.75\cdot10^{-9}$	16.2	16.2	527.4	0.007	30	49	62
15	1	Const. K	340	$1.50\cdot10^{-8}$	16.2	16.2	358.5	0.016	30	49	62
16a	1	Const. K	290	$6.78\cdot10^{-9}$	16.2	16.2	102.0	0.006	31	49	62
16b	1	Const. K	290	$6.14\cdot10^{-8}$	16.2	16.2	56.0	0.015	31	49	62
16c	1	Const. K	290	$4.17\cdot10^{-7}$	16.2	16.3	24.0	0.036	31	50	62
16d	1	Const. K	290	$4.87\cdot10^{-9}$	16.3	16.3	191.3	0.007	31	50	63

Table C-5 (continued) Crack growth rate data for Specimen B3CT03 (9.4 dpa) based on corrected (non-linear) DCPD data

Step	R ratio	Load[1] condition	Temp.[2] ºC	CGR[3] mm/s	K_{Istart} MPa$\sqrt{m}$[4]	K_{Istop} MPa$\sqrt{m}$[4]	Δt hours[5]	Δa mm[5]	K validity, %[6]		
									399	ΔYS/2	ΔYS/3
16e	1	Const. K	290	$5.09\cdot10^{-7}$	16.3	16.3	20.0	0.032	31	50	63
16f	1	Const. K	290	$1.52\cdot10^{-8}$	16.3	16.3	66.0	0.009	31	50	63
16g	1	Const. K	290	$2.61\cdot10^{-6}$	16.3	16.4	18.4	0.165	31	50	63
16h	1	Const. K	290	$1.66\cdot10^{-9}$	16.4	16.4	651.0	0.007	31	50	63
17a	1	Const. K	320	$1.27\cdot10^{-9}$	16.4	16.4	166.8	0.003	31	50	63
17b	0.6	9 ks hold	320	$2.59\cdot10^{-7}$	16.4	16.5	72.1	0.072	31	50	63
17c	1	Const. K	320	$1.45\cdot10^{-9}$	16.5	16.5	334.9	0.002	31	50	63
18[7]	0.2	1, dk/da=6	320	$6.22\cdot10^{-5}$	16.5	22.7	3.7	0.981	31	50	64
19[7]	0.4	1, dk/da=6	320	$3.99\cdot10^{-5}$	22.7	23.3	0.7	0.087	43	69	87
20[7]	0.4	0.3, dk/da=6	320	$1.45\cdot10^{-5}$	23.3	23.6	1.1	0.055	44	71	90
21[7]	0.4	0.1, dk/da=6	320	$4.45\cdot10^{-6}$	23.6	23.9	3.4	0.052	44	72	91
22[7]	0.4	0.03,	320	$1.79\cdot10^{-6}$	23.9	24.2	9.0	0.056	45	73	92
23[7]	0.4	0.01,	320	$5.72\cdot10^{-7}$	24.2	24.6	26.8	0.062	46	74	94
24[7]	0.4	0.003,dk/da=	320	$1.71\cdot10^{-7}$	24.6	24.9	96.0	0.059	47	76	95
25[7]	0.4	0.001,dk/da=	320	$7.09\cdot10^{-8}$	24.9	25.3	256.8	0.067	47	77	97
26[7]	0.5	0.001,dk/da=	320	$6.43\cdot10^{-8}$	25.3	25.7	277.8	0.068	48	78	99
27[7]	0.5	100s h,	320	$8.29\cdot10^{-8}$	25.7	26.1	227.3	0.072	49	80	100
28	0.5	1 ks hold	320	$5.35\cdot10^{-8}$	26.1	26.1	248.0	0.052	50	81	102
29	0.5	9 ks hold	320	$1.53\cdot10^{-8}$	26.1	26.2	312.8	0.022	50	81	103
30	1	Const. K	320	$2.87\cdot10^{-9}$	26.2	26.2	197.0	0.003	50	82	103

Table C-5 (continued) Crack growth rate data for Specimen B3CT03 (9.4 dpa) based on corrected (non-linear) DCPD data

Step	R ratio	Load[1] condition	Temp.[2] ºC	CGR[3] mm/s	K_{Istart} MPa√m[4]	K_{Istop} MPa√m[4]	Δt hours[5]	Δa mm[5]	K validity, %[6]		
									399	ΔYS/2	ΔYS/3
31	1	Const. K	340	$8.08 \cdot 10^{-9}$	26.2	26.2	285.4	0.003	50	82	103
32a	1	Const. K	290	$1.78 \cdot 10^{-8}$	26.2	26.2	36.5	0.009	50	82	103
32b	1	Const. K	290	$5.80 \cdot 10^{-6}$	26.2	28.4	56.6	1.234	50	82	103
32b1	1	Const. K	290	$1.59 \cdot 10^{-6}$	26.2	26.4	21.8	0.139	50	82	103
32b2	1	Const. K	290	$5.69 \cdot 10^{-6}$	26.4	27.1	20.9	0.446	51	83	105
32b3	1	Const. K	290	$1.21 \cdot 10^{-5}$	27.1	28.4	14.2	0.653	54	87	110
32c	1	dk/da=-4	290	$2.18 \cdot 10^{-5}$	28.4	28.1	11.3	0.904	58	94	118
32d	1	Const. K	290	$2.48 \cdot 10^{-5}$	28.1	30.9	10.7	0.941	60	97	123
32e	1	dk/da=-3	290	$2.31 \cdot 10^{-5}$	30.9	32.1	9.8	0.824	70	113	143
33a	1	dk/da=-3	320	$4.01 \cdot 10^{-5}$	32.0	37.0	12.2	1.759	76	124	156
33b	1	Const. K	320	$6.90 \cdot 10^{-5}$	37.0	41.9	2.5	0.602	101	164	207

1) Loading condition during testing. A number stands for the frequency in Hz during continuous cyclic load, whereas a number followed by a time and the word “hold” means the specimen was subjected to partial periodic unloading (PPU) with the hold time at maximum load indicated. Const. K or P means testing was conducted under constant stress intensity factor (K), or load (P), while ”dK/da=X” means K was changed by the nominal rate (in MPa√m/mm) indicated.
2) Test temperature during the step.
3) Crack growth rate determined by linear regression of the corrected DCPD curve.
4) Stress intensity factor based on the crack length corresponding to the first (K_{Istart}) and last (K_{Istop}) data point of the regression analysis and load data.
5) Difference in test time or crack length between the first and last data point of the regression analysis.
6) K validity according to ASTM E399 and modified criteria based on the same standard. An effective yield strength was used for the modified criteria, i.e., $YS_{eff1}=YS_{unirr} + (YS_{irr}-YS_{unirr})/2$ and $YS_{eff2}=YS_{unirr} + (YS_{irr}-YS_{unirr})/3$. The actual K during the step was related to the K limit based on the crack length when the step started, i.e., 100% or higher means the criterion was exceeded.
7) Positive dK/da as indicated plus continuous cycling at frequency and R ratio reported. “h” stands for hold time.

CGR Data from Halden

(reproduced from Tables 5 and 8 from HWR-1320 [5] and Table 7 from HWR-1236 [4])

Table C-6 Summary of crack growth rate data for CT1 from HWR-1320 (50 dpa)

Step	Time, hrs		Δt, hrs	CGR mm/s	K, MPa√m	Δa mm	K validity, %			Load
	start	stop					399	ΔYS/2	ΔYS/3	
1	5	53	48	1.21E-08	13.2	0.002	40	68	87	Constant
2	54	480	426	1.11E-08	14.6	0.017	45	75	97	Constant
3	654	980	326	1.04E-08	15.6	0.012	48	80	103	Constant
4	984	1084	100	2.60E-08	15.5	0.009	47	79	103	Cyclic
5	1090	1220	130	5.94E-09	15.7	0.003	48	81	104	Constant
6	1852	2164	312	3.06E-09	16.2	0.003	49	83	107	Constant
7	2166	2360	194	-3.10E-09	17.6	-0.002	54	90	117	Constant
8	2360	2740	380	1.68E-08	18.6	0.023	57	95	123	PPU
9	2908	3264	356	2.64E-08	20.6	0.034	63	106	136	PPU
10	4420	4776	356	5.55E-09	20.7	0.007	63	106	137	PPU
11	4780	5560	780	1.90E-08	22.9	0.053	70	117	152	PPU
12	5570	5880	310	3.74E-08	24.8	0.042	76	127	164	PPU
13	5892	5920	28	3.28E-07	25.0	0.033	76	128	166	PPU
14	7040	7170	130	1.24E-07	26.6	0.058	81	136	176	PPU
15	7180	7244	64	5.80E-07	27.8	0.134	85	143	184	PPU
16	7560	7800	240	2.38E-07	29.8	0.206	91	153	197	PPU
17	7800	8520	720	1.28E-07	31.6	0.332	96	162	209	PPU
18	8580	8810	230	1.35E-07	33.9	0.112	103	174	225	PPU

Table C-7 Summary of crack growth rate data for CT4 from HWR-1320 (40 dpa)

Step	Time, hrs		Δt, hrs	CGR mm/s	K, MPa√m	Δa mm	K validity, %			Load
	start	stop					399	ΔYS/2	ΔYS/3	
1	5	53	48	1.49E-08	13.2	0.003	40	68	87	Constant
2	53	480	427	9.58E-09	14.5	0.015	44	74	96	Constant
3	654	980	326	7.37E-09	15.5	0.009	47	79	103	Constant
4	984	1084	100	2.67E-08	15.4	0.010	47	79	102	Cyclic
5	1090	1220	130	8.45E-09	15.6	0.004	48	80	103	Constant
6	1852	2164	312	8.55E-10	16	0.001	49	82	106	Constant
7	2166	2380	214	-5.22E-09	17.5	-0.004	53	90	116	Constant
8	2380	2740	360	1.74E-08	18.5	0.023	56	95	123	PPU
9	2908	3264	356	7.84E-08	20.6	0.100	63	106	136	PPU
10	4420	4776	356	3.22E-08	21	0.041	64	108	139	PPU
11	4778	4790	12	1.09E-05	23.8	0.471	73	122	158	PPU
12	4790	4798	8	2.48E-05	24.8	0.714	76	127	164	PPU
13	4798	4802	4	3.82E-05	31.4	0.550	96	161	208	PPU
14	4802	4808	6	1.86E-05	29.2	0.402	89	150	193	PPU

Table C-8 Summary of crack growth rate data for CT4 from HWR-1236 (41 dpa)

Step	Time, hrs		Δt, hrs	CGR mm/s	K, MPa√m	Δa mm	K validity, %		
	start	stop					399	ΔYS/2	ΔYS/3
1	362.5	371	8.5	1.72E-05	11.73	0.53	35.8	60.2	77.7
2	371	380	9	9.18E-06	12.6	0.30	38.4	64.6	83.4
3	380	492	112	2.34E-07	13.16	0.09	40.1	67.5	87.2
4	492	560	68	2.64E-06	13.81	0.65	42.1	70.8	91.5
5	560	593	33	5.03E-06	14.47	0.60	44.1	74.2	95.8
6	593	611	18	1.18E-06	14.7	0.08	44.8	75.4	97.4
7	611	711	100	2.06E-07	14.91	0.07	45.5	76.5	98.7
8*	717	876	159	6.02E-08	14.84	0.03	45.2	76.1	98.3
9	1071	1110	39	1.37E-06	15.99	0.19	48.8	82.0	105.9
10	1110	1122	12	4.83E-06	16.8	0.21	51.2	86.2	111.3
11	1122	1140	18	1.64E-05	17.38	1.06	53.0	89.1	115.1
12	1160	1288	128	1.19E-07	11.52	0.05	35.1	59.1	76.3
13	1328	1672	344	5.30E-08	11.89	0.07	36.3	61.0	78.7

* shaded row indicates data generated in hydrogen water chemistry. Remaining data generated in normal water chemistry

CGR Data from ANL

(reproduced from Table 9 of ANL-19/45 [6])

Table C-9: SCC CGR test results for the decommissioned Zorita baffle plate materials

Sample ID.	Dose (dpa)	Test Env.	SCC CGR		
			K (MPa√m)[a]	**CGR with PPU** (×10^{-8} mm/s)	**CGR w/o PPU** (×10^{-8} mm/s)
A3CT04	~0.06	PWR	15.5	0.99	-
			15.6	-	0.05
			21.5	1.51	-
			21.6	-	0.38
			27.5	1.77	-
			27.5	-	0.20
B3CT14	~8	Low-DO, high-purity	16.9	2.43	-
			17.2	-	1.47
			21.2	2.86	-
			21.2	-	1.78
			27.0	1.71	-
			27.0	-	1.27
ACT03	~15	Low-DO, high-purity	16.4	1.00	-
			16.4	-	0.96
			20.7	1.35	-
			20.7	-	0.59
			26.5	3.74	-
			26.9	-	2.25
B1CT07	~39	Low-DO, high-purity	16.7	3.03	-
			17.1	-	1.84
			21.3	3.01	-
			21.1	-	1.82
			26.0	3.94	-
			26.2	-	1.47
B1CT09	~47	Low-DO, high-purity	16.4	1.20	-
			16.6	-	0.80
			20.1	1.75	-
			20.2	-	1.24
			25.2	2.46	-
			25.3	-	1.04
B1CT08	~47	PWR	19.8	1.88	-
			19.8	-	0.90
			23.9	2.19	-
			24.4	-	409
			24.5	-	49.2
			24.3-26.0	-	906
			26.0-29.2	-	4290
			5.5	-	1.5
			17	-	0.40
			30-39.0	-	4280
			32.7-37.0	-	5780
			25.3-30.9	-	5350
			10.9	-	2.33
			66.5-77.6	-	4340

[a]When a rising K condition is present, a K range is provided.

APPENDIX D: ADDITIONAL REFERENCES FOR SELECTED FIGURES

This appendix contains additional references to correlate with the citations shown in Figures 10, 12, A-1, A-2, A-3, and B-1.

For Figures 10, 12, and B-1, the following references from MRP-451 are:

2. Electric Power Research Institute, "Materials Reliability Program: Zorita Internals Research Project (MRP-440), Testing of Highly-Irradiated Baffle Plate Material," Product ID 3002016015, Palo Alto, CA, October 29, 2019 (proprietary; available for viewing through the NRC Technical Library[6]).

6. Jenssen, A. J. Stjärnsäter, K. Kese, R. Carter, J. Smith, A. Demma, and M. Hiser, "Fracture Toughness Testing of an Irradiated PWR Core Barrel Weld," Fontevraud 9—Contribution of Materials Investigations and Operating Experience to LWRs' Safety, Performance and Reliability, Avignon, France, September 17–20, 2018.

8. Electric Power Research Institute, "BWRVIP-154, Revision 2: BWR Vessel and Internals Project, Fracture Toughness in High Fluence BWR Materials – Final Report," Product ID 1019077, Palo Alto, CA, 2009.

16. Electric Power Research Institute, "BWRVIP-221: BWR Vessel and Internals Project, Crack Growth in High Fluence BWR Materials – Crack Growth Rate Testing of Types 304L and 316L at doses ranging from 3.5 to 13 dpa," Product ID 1019079, Palo Alto, CA, 2009.

18. A. Jenssen, R. Pathania, R. Carter, "Crack Growth in Irradiated Austenitic Stainless Steels in BWR Environments," Fontevraud 8 - Contribution of Materials Investigations and Operating Experience to LWRs' Safety, Performance and Reliability, Avignon, France, September 2014.

30. A. Jenssen, J. Stjärnsäter, R. Pathania, R. Carter, "Crack Growth in Irradiated Stainless Steel Welds in BWR Environments," Fontevraud 9 - Contribution of Materials Investigations and Operating Experience to LWRs' Safety, Performance and Reliability, Avignon, France, September 2018.

31. Electric Power Research Institute, "Materials Reliability Program: A Review of Radiation Embrittlement of Stainless Steels for PWRs (MRP-79) – Revision 1," Product ID 1008204, Palo Alto, CA, 2004.

32. A. Demma, R. Carter, A. Jenssen, T. Torimaru, R. Gamble, "Fracture Toughness of Highly Irradiated Stainless Steels in Boiling Water Reactors," 13th International Symposium on Environmental Degradation of Materials in Nuclear Power Systems—Water Reactors, Whistler, BC, Canada, August 2007.

50. U. Ehrnstén, K. Wallin, P. Karjalainen-Roikonen, S. van Dyck and P. Ould, "Fracture Toughness of Stainless Steels Irradiated up to ~9 dpa in Commercial BWRs," Fontevraud 6—Contribution of Materials Investigations to Improve the Safety and Performance of LWRs, Fontevraud, France, September 2006.

For Figures A-1, A-2, and A-3, the following references from MRP-440 are:

11. Electric Power Research Institute, “BWRVIP-154, Revision 2: BWR Vessel and Internals Project, Fracture Toughness in High Fluence BWR Materials – Final Report,” Product ID 1019077, Palo Alto, CA, 2009.

16. A. Jenssen, P. Efsing, B. Forssgren, B. Bengtsson and M. Molin, “Examination of Highly Irradiated Stainless Steels from BWR and PWR Reactor Pressure Vessel Internals,” Fontevraud 7—Contribution of Materials Investigations to Improve the Safety and Performance of LWRs, Avignon, France, September 2010.

20. Electric Power Research Institute, “BWRVIP-221: BWR Vessel and Internals Project, Crack Growth in High Fluence BWR Materials – Crack Growth Rate Testing of Types 304L and 316L at doses ranging from 3.5 to 13 dpa,” Product ID 1019079, Palo Alto, CA, 2009.

33. A. Jenssen, R. Pathania, R. Carter, “Crack Growth in Irradiated Austenitic Stainless Steels in BWR Environments,” Fontevraud 8 - Contribution of Materials Investigations and Operating Experience to LWRs’ Safety, Performance and Reliability, Avignon, France, September 2014.

36. Electric Power Research Institute, “Models of Irradiation-Assisted Stress Corrosion Cracking of Austenitic Stainless Steels in Light Water Reactor Environments: Volume 2 Disposition Curves Application,” Product ID 3002003103, Palo Alto, CA, 2014.

40. A. Jenssen, J. Stjärnsäter, R. Pathania, R. Carter, “Crack Growth in Irradiated Stainless Steel Welds in BWR Environments,” Fontevraud 9 - Contribution of Materials Investigations and Operating Experience to LWRs’ Safety, Performance and Reliability, Avignon, France, September 2018.

41. Electric Power Research Institute, “Materials Reliability Program: A Review of Radiation Embrittlement of Stainless Steels for PWRs (MRP-79) – Revision 1,” Product ID 1008204, Palo Alto, CA, 2004.

42. A. Demma, R. Carter, A. Jenssen, T. Torimaru, R. Gamble, “Fracture Toughness of Highly Irradiated Stainless Steels in Boiling Water Reactors,” 13th International Symposium on Environmental Degradation of Materials in Nuclear Power Systems—Water Reactors, Whistler, BC, Canada, August 2007.

43. Grönwall, B, Birath, S, Haag, Y. “Ringhals 1, System 216-Hot Cell Examination of a SRM/IRM (dry tube) Guide Tube Manufactured by General Electric – Final Report” (in Swedish), STUDSVIK/NS-89/75, Studsvik Nuclear AB, Sweden, 1989.

44. A. Jenssen, V. Grigoriev, R. Jakobsson, P. Efsing, ”Fracture Resistance Evaluation of a Flux Thimble Irradiated to 65 dpa in a PWR,” Fontevraud 6—Contribution of Materials Investigations to Improve the Safety and Performance of LWRs, Fontevraud, France, September 2006.

45. Conermann, J, Shogan R. P, Forsyth, D. R, Wilson, I. L, Tang, H. T, “Characterization of Baffle-Former Bolts Removed from Service in US PWRs”, 10th International Symposium on Environmental Degradation of Materials in Nuclear Power Systems—Water Reactors, Lake Tahoe, NV, August 2001.

48. R. W. Bosch, M. Vankeerberghen, R. Gérard, F. Somville, “Crack initiation testing of thimble tube material under PWR conditions to determine a stress threshold for IASCC,” Journal of Nuclear Materials. 461, pp. 112–121, 2015.

49. Electric Power Research Institute, “Materials Reliability Program: Effect of Lithium on IASCC Initiation (MRP-413),” Product ID 3002008082, Palo Alto, CA, 2016.

51. Electric Power Research Institute, “Materials Reliability Program: Characterizations of Type 316 Cold Worked Stainless Steel Highly Irradiated Under PWR Operating Conditions (International IASCC Advisory Committee Phase 3 Program Final Report) (MRP-214),” Product ID 1015332, Palo Alto, CA, 2007.

52. K. Takakura, K. Nakata, M. Ando, K. Fujimoto and E. Wachi, “Lifetime Evaluation for IASCC Initiation of Cold Worked 316 Stainless Steel’s BFB in PWR Primary Water,” 13th International Symposium on Environmental Degradation of Materials in Nuclear Power Systems—Water Reactors, Whistler, BC, Canada, August 2007.

53. H. Nishioka, K. Fukuya, K. Fujii, T. Torimaru, “IASCC properties and mechanical behavior of stainless steels irradiated up to 73dpa,” 13th International Symposium on Environmental Degradation of Materials in Nuclear Power Systems—Water Reactors, Whistler, BC, Canada, August 2007.

54. T. M. Karlsen, M. Espeland, H. Jenssen, “Crack Initiation in Irradiated Constant Load Tensile Specimens using Off-line Instrumentation – Results from First and Second Loadings,” Institutt for Energiteknikk, Norway, 2007, FC Note 1545. Available on: Cooperative IASCC Research II Program: Final Comprehensive CIR II CD Version 10.08, Product ID 1021235, EPRI, Palo Alto, CA, 2010.

55. C. Pokor, A. Toivonen, M. Wintergerst, U. Ehrnstén, W. Karlsen, J-P. Massoud, “Determination of the Time to Failure Curve as a Function of Stress for a Highly Irradiated AISI 304 Stainless Steel after Constant Load Tests in Simulated PWR Water Environment,” Fontevraud 7—Contribution of Materials Investigations to Improve the Safety and Performance of LWRs, Avignon, France, September 2010.

63. J. Nakano, T.M. Karlsen, M. Espeland, ”Summary of Results from the PWR Crack Growth Rate Investigation IFA-670,” OECD Halden Reactor Project, Report HWR-843, August 2008.

66. U. Ehrnstén, K. Wallin, P. Karjalainen-Roikonen, S. van Dyck and P. Ould, ”Fracture Toughness of Stainless Steels Irradiated up to ~9 dpa in Commercial BWRs,” Fontevraud 6—Contribution of Materials Investigations to Improve the Safety and Performance of LWRs, Fontevraud, France, September 2006.